

Bending and Shear Improvements in 3D-printed Core Sandwich Composites through Modification of Resin Uptake in the Skin/Core Interphase Region

Dongyang Cao¹, Dan Bouzolin¹, Hongbing Lu¹, D. Todd Griffith^{1,*}

¹ Department of Mechanical Engineering, The University of Texas at Dallas, Richardson, TX 75080, USA

* Corresponding author. E-mail address: tgriffith@utdallas.edu

ABSTRACT

Fused deposition modeling (FDM) printed polymers are rarely used as a structural material due to anisotropic and low mechanical properties compared with conventional composites. In recent years, greater need has been expressed for recycling of materials, such as recyclable FDM, at the end of service life to reduce environmental pollution and manufacture cost. However, how the amount of resin uptake in the skin and skin/core interphase affects the bending and shear performance of the sandwich composites when replacing the low strength and ductile core (conventional core) with a high strength and brittle core (FDM printed PLA (polylactic acid) core) still remains unclear. A new manufacturing routine is needed to improve the incorporation of FDM printed polymers in composite structures. In this work, FDM printed PLA was used as core material and sandwiched between two unidirectional glass fiber reinforced polymer (GFRP) skins to form a sandwich composite by compression-molding (CM) process, which provides a good manufacturing strategy for skin/core interphase modification. The significance of the CM process is proved by investigating the effect of resin uptake on bending and in-plane/out-of-plane shear performances. Current first order shear deformation (FSDT) theory lacks a direct connection between the in-plane shear stress and out-of-plane shear stress in the core region of sandwich composites. With the help of DIC, a connection between the in-plane shear and the out-of-plane shear strain was built and in-plane shear properties can acquire through out-of-plane shear properties, hence reducing the redundancy of sample preparation or the need for simulation. A significant improvement was found compared with the optimized resin uptake (Optimized resin uptake range: 20.43% ~ 22.86 wt%) 3D-printed PLA core sandwich composite and lowest performance sandwich composite (Improvement: in-plane shear strength (~34%)/modulus (~29%), out-of-plane shear strength (~25%)/modulus (~31%), specific peak bending load (~19%). Compared with balsa core sandwich composites, the 3D-printed cores are suitable for use in composite sandwich structures in many applications with a satisfactory strength-to-weight ratio.

KEYWORDS

Fused deposition modeling, 3D-printed core sandwich composite, sustainable structure, skin/core interphase, first-order shear deformation theory, low carbon emission

1. INTRODUCTION

Based on the investigation of the World Bank Group, over 1.3 billion tons of solid waste were produced on the whole global earth per year, and this trend will be increased to at least 2.2 billion tons by the year 2025^{1,2}. To overcome the serious environmental pollution issue coming from aerospace, automotive, and constructions, thermoplastic matrix composites have received increased attention due to their characteristics including recyclability, eco- and environmentally-friendly nature, thermoformability, and comparable stiffness to the thermoset matrix composites^{3,4}. The fused deposition modeling (FDM) process is one of the most common ways to fabricate thermoplastics with rapid-prototyping, complex geometries, and infill by topology optimization through CAD type software^{5,6}. One of the FDM processes, fused filament fabrication (FFF) has recently attracted the attention of many researchers due to a potential match with conventional composites. Blok et al. claimed that the continuous carbon fiber/nylon-6 matrix composites fabricated by FFF possess tensile strength and modulus of 986 MPa and 62.5 GPa, flexural strength and modulus of 485 MPa and 41.6 GPa, shear strength and modulus of 31.16 MPa and 2.26 GPa with ~27% fiber volume fraction (FVF)⁷. Matsuzaki et al. state that, continuous carbon fiber/chopped jute fiber PLA matrix composite fabricated by FFF possesses tensile strength

and modulus of 40~185 MPa and 4~20 GPa, respectively under ~6% FVF⁸. Although many works are dedicated to void elimination on the matrix and the mechanical properties are compatible with conventional composites, there are still many limitations to this routine, like poor layer adhesion led to anisotropic structure, induced thermal residual stress, and poor fiber to matrix bonding. These limitations lead to poor fiber usage efficiency and incredibly high cost due to a higher volume demand for fiber compared with conventional fabrication for engineering structure construction. Due to the existing limitations, this work will explore the feasibility of the 3D-printed thermoplastic polymer lattices for use as cores for sandwich composites. Attention is focused on the out-of-plane shear properties through the cross-section of sandwich composites and in-plane shear properties along the lengthwise of the FDM printed core determined from three-point bending and four-point bending tests.

Sandwich composites with skins bonded on both sides of a lightweight core are usually used in applications that require high strength or stiffness-to-weight ratio in the civil, marine, and aerospace industry⁹⁻¹². Core materials such as balsa wood, polyvinyl chloride (PVC), polyethylene terephthalate (PET), and polyurethane (PU) foam are often used due to a high buckling load, high energy absorption, high shear stiffness, ease of machining, and recyclability¹³⁻¹⁶. In the design of the sandwich structure, one of the critical considerations is that the core should provide a sufficiently high shear stiffness to prevent buckling¹⁷⁻¹⁹. In recent years, 3D-printed lattice cores have been used as the core material in sandwich composites²⁰. Li et al. reported that the carbon fiber skin with 3D-printed lattice and honeycomb core sandwich composites provide sufficient flexural (3.98~12.94 MPa) and shear strengths at a relatively low density (0.2~0.4 g/cm³)²¹. Ye et al. reported the compressive strengths (0.95~4.08 MPa) and specific energy absorption (10~19 J/g) for the 3D-printed PLA pyramidal lattices with different aspect ratios²². Xu et al. determined that the 3D-printed honeycomb core, fabricated by selective laser sintering (SLS) of glass fiber-filled polyamide-12 powder, has reached a satisfactory critical buckling strength (3~12 MPa)²³. All the previously reported results on 3D-printed cores have stressed the importance of core topology, wall thickness, and infill density on the core mechanical performance in increasing the strength and stiffness while reducing the weight²⁴. To date, it is still inconclusive whether 3D-printed lattice cores can replace the conventional cores in sandwich composites in engineering structures, such as wind turbine blades, due to the limitations and defects that arise from FDM fabrication. This paper will investigate the mechanical performance of 3D-printed core composites and compare it with that of the conventional core composites. To this end, 3D-printed core composites are fabricated and tested.

Resin uptake represents the amount of resin absorbed as a fraction of the entire sandwich composite. The core volume, topology, and resin infiltration time are factors that influence resin uptake²⁵⁻²⁷. The skin/core interphase is the place where fracture initiates on the sandwich structure, so a sufficient amount of resin is needed in this area to prevent crack formation²⁸. While the resin is required to infiltrate into the skin/core interphase region to bond the skin and core, an unnecessarily high resin uptake in the sandwich composite leads to increased cost and weight²⁹. Therefore, reducing resin uptake of sandwich composites is essential to reduce weight, increase structural stability, and ultimately reduce costs (such as the Levelized Cost of Energy (LCOE) in the wind energy application³⁰. However, to the best of our knowledge, an appropriate range of resin uptake has yet to be determined for the FDM printed core sandwich composite based on the bending and shear performances²⁹. We vary the amounts of resin uptake through CM process in a 3D-printed core sandwich composite and compare both the shear strength and shear stiffness with the corresponding values in a conventional core sandwich composite.

Compression-molding (CM) is a conventional composite fabrication approach that is relatively clean, has low resin consumption, and has low labor costs³¹. In the last decade, the CM process has emerged as a common composite manufacturing process with high efficiency and ease of automation. In the CM process, the amount of resin uptake of the sandwich composite can be readily controlled by adjusting the compression pressure; whereas in the vacuum-assisted resin transfer molding (VARTM) process³², the amount of resin uptake is difficult to change as the vacuum pressure is nearly constant.

In this paper, we investigate how resin uptake affects the shear strength and shear stiffness of the PLA lattice core composites, and compare the results with the corresponding values of the conventional core composites, specifically, H60 PVC foam core and balsa core sandwich composites. The flexural properties per unit weight of the composite and cost analysis of eleven 3D-printed materials and infill settings are provided. Two types of conventional cores, H60 non-perforated smooth core (PSC) and PVC core are used to fabricate the conventional core composites. The PLA cores are made at 15% infill density and tetrahedral infill pattern. The PLA cores are bonded to glass fiber epoxy composite skins at various amounts of resin uptake by the CM process. The effects of the amount of resin uptake on both the in-plane and the out-of-plane shear strength and shear stiffness in the core sandwich composites are investigated. The surface strain distributions of two types of cores (3D-printed and H60 PVC) sandwich composites are determined by digital image correlation (DIC) to identify the vulnerable region of the composite under bending. The failure modes for the sandwich composites are observed. A detailed comparison was made between recyclable materials and our work in the discussion section to fully insight the future trend of green sandwich composite fabrication and material selections.

2. METHODS

The procedures for the preparation of the PLA and conventional core sandwich composites and the details on the experimental characterization of the mechanical properties in bending are described in this section.

2.1 Materials

Three common commercially available filaments in 1.75 mm diameter were used in 3D printing. The first type of filament is a thermoplastic polymer consisting of polylactic acid (PLA) and acrylonitrile butadiene styrene (ABS) (Craftbot, Carrollton, TX). The second type of filament is chopped fiber-filled thermoplastic polymers; they include carbon fiber/PLAs, copper fiber/PLA, brass fiber/PLA, carbon fiber/ polyethylene terephthalate (PETG), glass fiber/polypropylene (PP) (Craftbot, Carrollton, TX) (3DXTECH, Grand Rapids, MI). The third type of filament is fiber/thermoplastic polymer consisting of continuous carbon fiber/onyx (chopped carbon fiber/nylon) (Markforged, Watertown, MA). These filaments were used to investigate the effect of the infill pattern, infill density, and core material type on the mechanical properties of the sandwich composites.

PVC foams (Divinycell™ H60; Diab Group, DeSoto, TX) were used as the conventional cores; they are lightweight with higher flexibility than a balsa wood³³. The as-received foams have dimensions of 121.92 × 121.92 × 2.54 cm. They were cut using a water-jet to 254 × 50.8 × 12.7 mm. Unidirectional glass fiber fabric (UD 970, Saertex, LLC, Huntersville, NC) with a measured aerial density of 957 g/m² and 1 mm densified thickness was used to embed in the epoxy matrix (EPIKOTE™ Resin MGS® RIMR 135; EPIKURE™ Curing Agent MGS® RIMH 1366, Hexion, Inc., Columbus, OH) to fabricate the composite skins. The epoxy resin used exhibits a low viscosity at room temperature and can be cured at room temperature. Two breathing films (Polyester; FibreGlast, Brookville, OH), and two release films (Fluorinated ethylene propylene; FibreGlast, Brookville, OH) were used in the CM process.

2.2 3D printing (FDM) process

The schematic of the fused deposition modeling (FDM) process is shown in Fig. 1. Craftbot 3 fused deposition modeling (FDM) dual extrusion 3D printer (Craftbot, Carrollton, TX) was used to print the thermoplastic and chopped fiber/thermoplastic specimens. The printing speed was set at 30 mm/s. A 0.4 mm diameter stainless steel nozzle and 0.3 mm layer height were used to achieve a smooth surface. The nozzle and bed temperatures were set to 215 °C and 60 °C, respectively. The infill density varied from 15%, 30%, 40%, and 80% for PLA. The initial deposition layer angle and the subsequent deposition layer angles of the PLA beams were set to 0 degrees (initial) and 0, 15, 30, 45, 60, 75, and 90 degrees (increment), respectively. Both the initial and increment angles of the deposition layer of the composite skins of the 3D-printed core composite beams were set to 0°. Several infill patterns were chosen to evaluate the effect of the infill pattern on the bending stiffness of the 3D-printed beams and details are shown in Fig. 2.

The Mark II FDM dual nozzle system 3D-printer (Markforged, Watertown, MA) was used to print the

continuous carbon fiber skin/onyx core specimens. The onyx matrix mainly consists of polyamide-6. The printing temperature of the onyx and carbon filaments were set at 275 and 250 °C, respectively. In addition, the printing speed was set to 10 mm/s. The layer height was set to 0.125 mm. The thickness of both top and bottom wall shells was set to 0.5 mm (deposited layer number: 4; increment angle: $-45^{\circ}/+45^{\circ}$); the thickness of all side walls was set to 0.8 mm. For the continuous fiber specimens, the lower bound of the infill density was set to 30%; then the upper bound of the infill density was set to the maximum infill density (tetrahedral: 55%, rectangular: 62%, and hexagonal: 92%). The continuous solid infill pattern can reach an adjustable infill density of up to 100%. Four continuous carbon fiber layers were inserted between the top and bottom skins. The orientation of the carbon fiber layers was $[0^{\circ}/45^{\circ}/90^{\circ}/135^{\circ}]$. The infill patterns in the continuous carbon fiber and onyx are shown in Figs. 3 and 4.

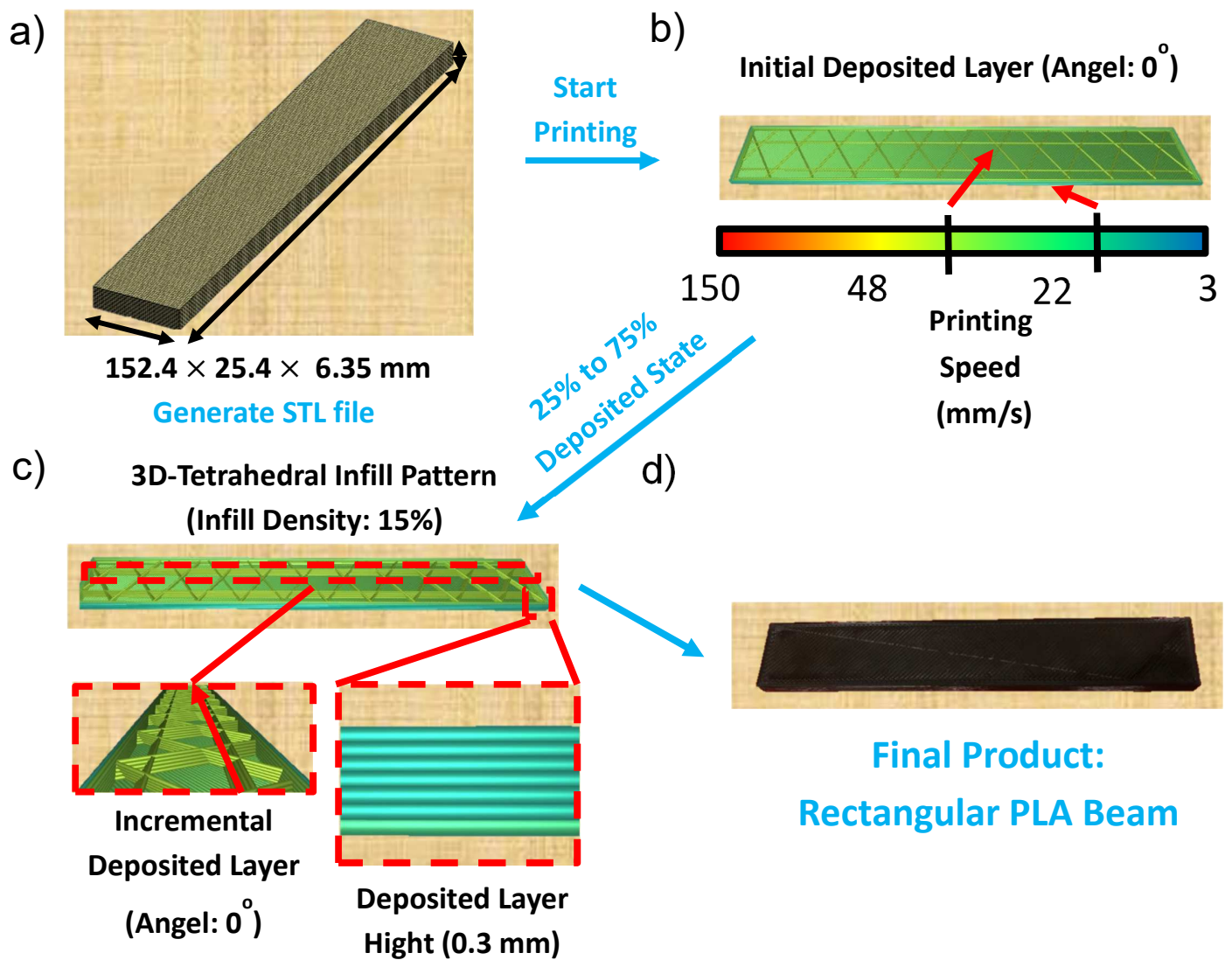


Figure 1: Schematic of the FDM process; a) 3D Isomeric view of the rectangular PLA beam before sliced into a G-code; b) Initially deposited layer with 0° initial deposited orientation (Note: printing speed at wall region: 15 mm/s, infill region: 30 mm/s); c) Sectional view of 75% deposited state rectangular PLA beam with 0° deposited layer incremental orientation (Note: deposited layer height: 0.3 mm); d) Finished 3D-printed PLA rectangular beam.

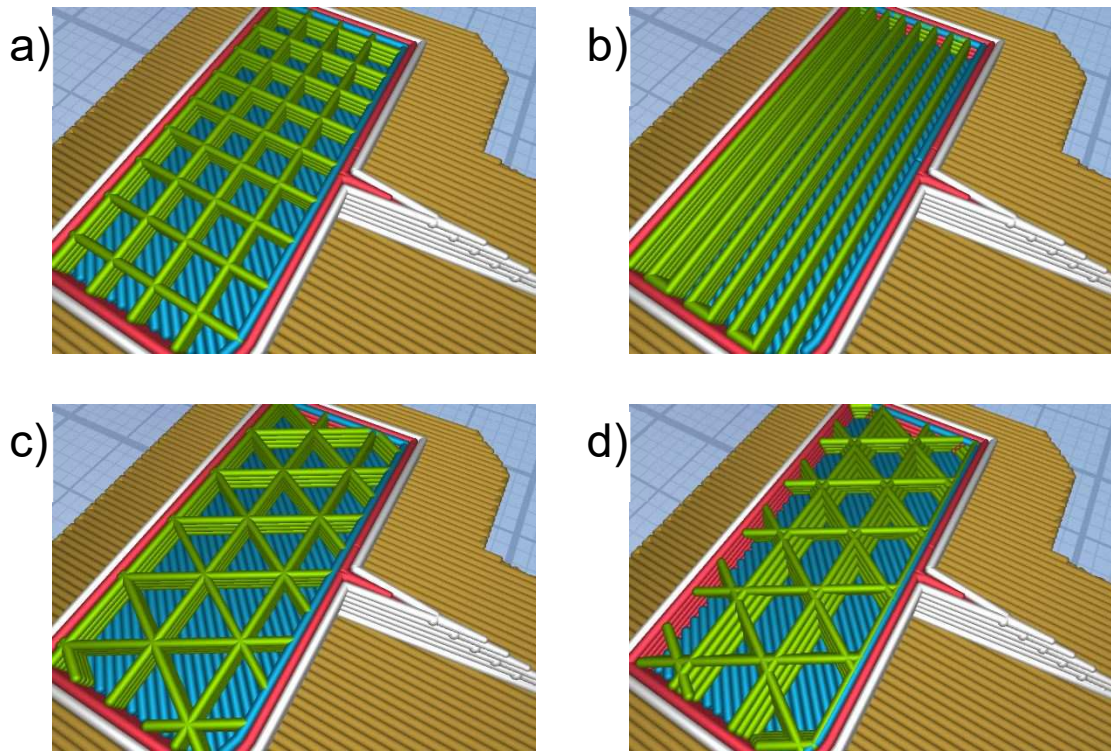


Figure 2: Four infill patterns of the PLA beams ($152.40 \times 25.40 \times 6.35$ mm): a) 40%-square infill pattern; b) 40%-parallel infill pattern; c) 40%-2D tetrahedral infill pattern; d) 40%-3D tetrahedral infill pattern.

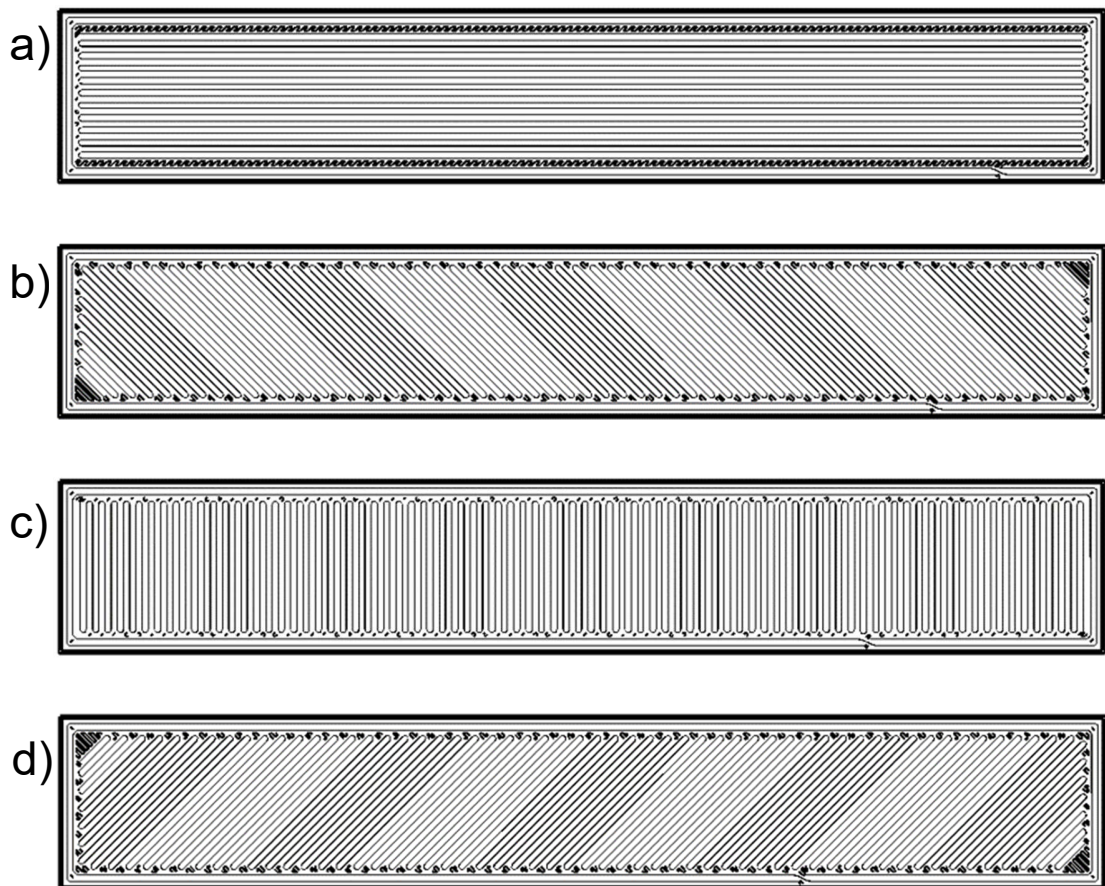


Figure 3: The infill patterns in the continuous carbon fiber layers in the 3D-printed beams: a) the first deposited layer at layer orientation of 0° ; b) the second deposited layer at layer orientation of -45° ; c) the third deposited layer at layer orientation of 90° ; d) the fourth deposited layer at layer orientation of 45° .

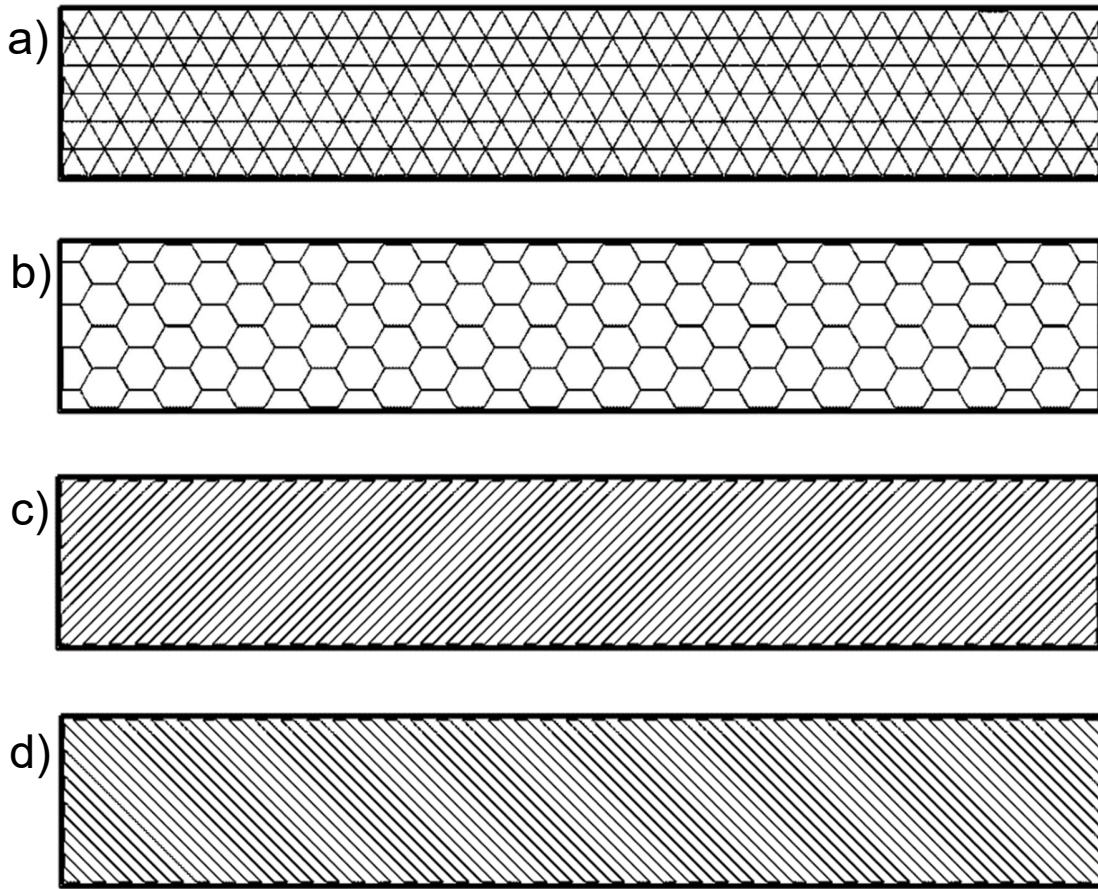


Figure 4: The infill patterns in the onyx (chopped carbon fiber/polyamide-6) layers in 3D-printed beams: a) 30% tetrahedral infill; b) 30% hexagonal infill; c) 45° parallel patterns of rectangular and solid infill; d) -45° parallel patterns of rectangular and solid infill.

2.3 Compression-molding of the sandwich specimens

A schematic of the compression-molding (CM) setup for the sandwich composites is shown in Fig. 5. PVC foams were cut, using a water jet, into the desired core geometry. Subsequently, the cores were cleaned with ethanol and dried with compressed air for one hour under ambient conditions. The 3D-printed PLA core (15%-infill density, 3D-tetrahedral infill pattern) was used directly after 3D printing. Epoxy and curing agent were mixed at a 10:3 w/w ratio for 10 minutes at room temperature and set for 5 minutes until no visible bubbles were observed. Then the resin mixture was put in the vacuum chamber for 20 minutes degas. The release film, breathing cloth, glass fabric, and core (PVC foam and 3D-printed core) were laid down in sequence. The epoxy mixture was poured gently on the fiber fabric and the core until the skins and core were fully saturated, then kept at 50°C for 1.5 hrs to avoid voids formation. The sandwich composites were cured for one day at room temperature to reach a partially cured state. Then, a second-stage cure was conducted in an autoclave for 4 hours at 80°C to achieve a fully cured state. Three different pressures (164, 197, and 230 kPa) were applied to each type of sandwich composite to prepare specimens with different amounts of resin uptake. Pictures of the sandwich composites with a foam core and a 3D-printed core are shown in Fig. 6.



Epoxy Resin/Hardener Mixer
(W:W/10:3)



Degas: 20 minutes under vacuum.
(Vacuum Level: 25.5" Hg)

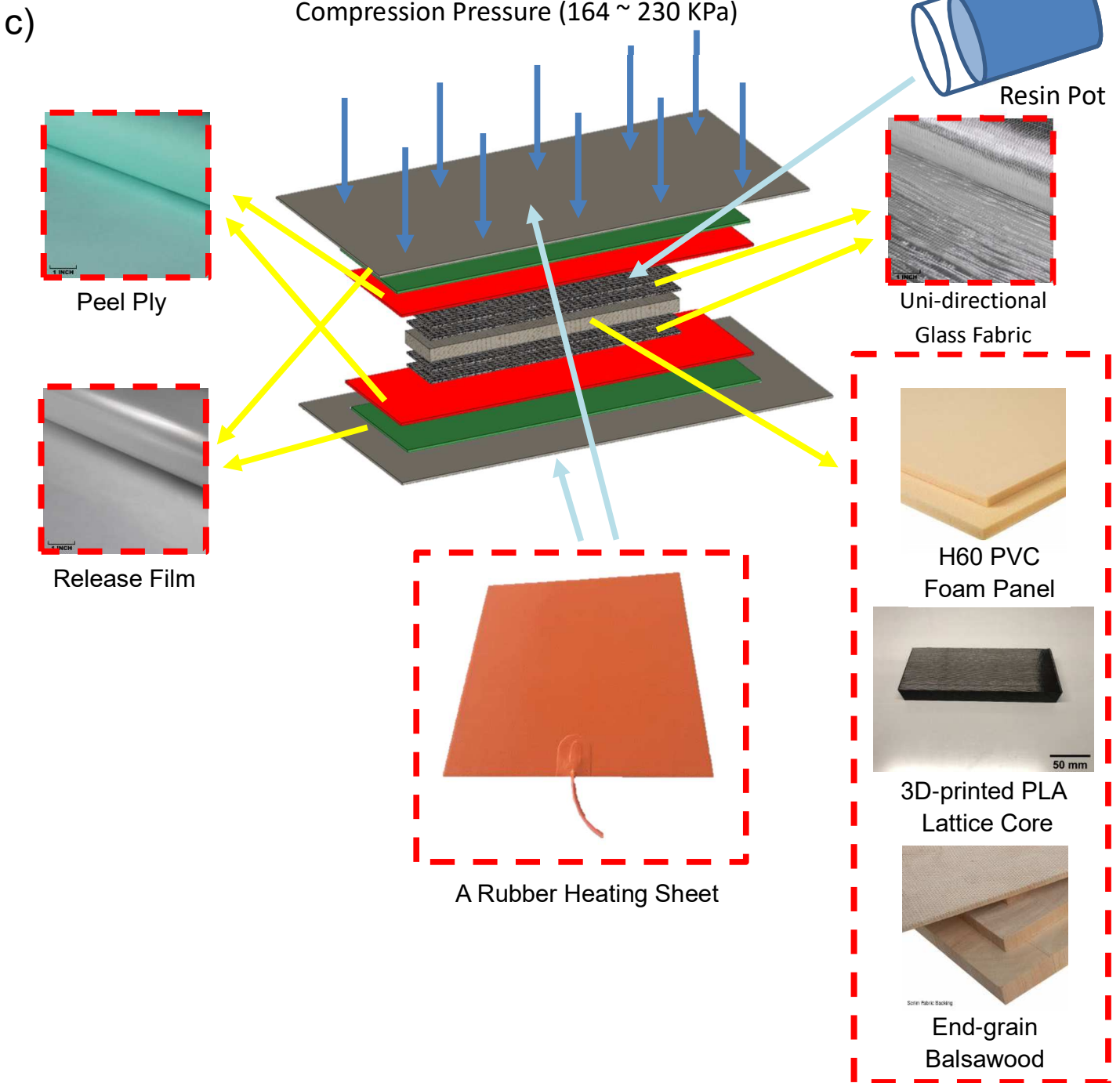


Figure 5: Schematic of the compression-molding setup and process: a) resin mixing and processing (Mixing time: 10 minutes); b) Resin mixture degassing process (Degas time: 20 minutes); c) compression-molding process (Note: skin thickness: ~2 mm; core thickness: ~12.7 mm).

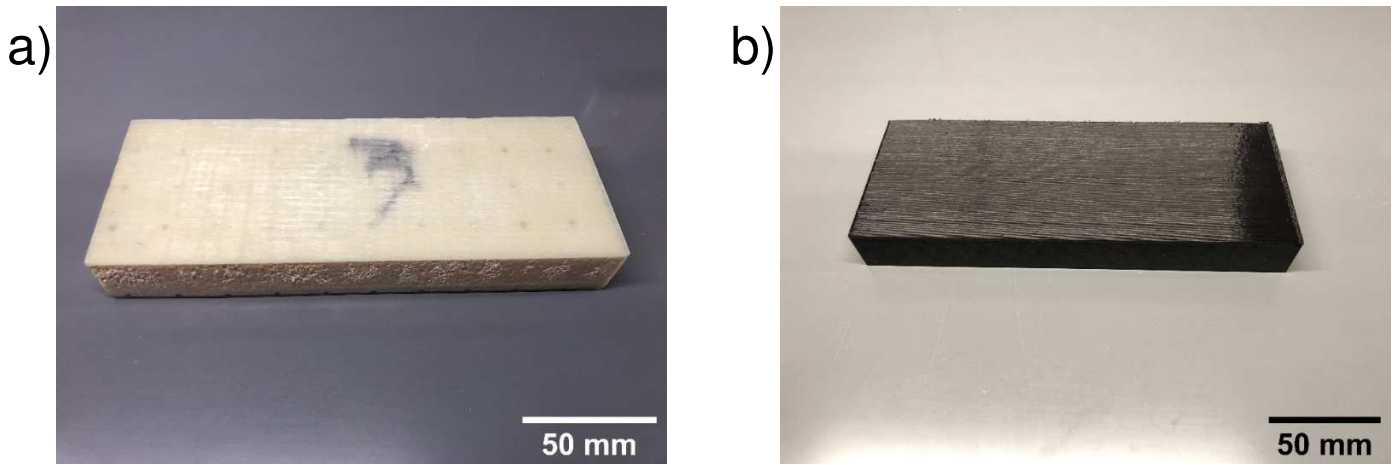


Figure 6: Pictures of core sandwich composites: a) a H60 PVC foam core glass fiber composite plate; b) a PLA lattice core.

2.4 Four-point bending tests

Following the ASTM C393 standard³⁴, the in-plane shear strength and stiffness of the sandwich composites were measured. The specimen dimensions, number of specimens, and crosshead speed used in experiments followed the ASTM D790. The loading span was 50.8 mm. A support span to depth ratio of 8:1 was used^{34,35}. As for the numerical values and specifications of the three-point bending tests used in this paper were previously investigated²⁹. It is noted that it is difficult to reach identical specimen configurations due to manufacturing deviation, when the resin uptake difference in two specimens is around 1%, the two specimens are considered equivalent.

2.5 The digital image correlation (DIC) technique

The digital image correlation (DIC)⁴⁴⁻⁴⁷ was used to measure the deformations of the side surface of a specimen using the 2D GOM Correlate software (GOM Inc., Charlotte, NC). During a three-point bending, images of the specimen surface were acquired every 1 s using a Nikon D7100 camera with 3840×2748 pixel resolution and a 24 mm Nikon lens. A NiLA VARSA LED light was used for illumination. The camera work distance was 1.3 m; it allowed us to capture images of the specimen in the entire support span.

3. CALCULATION OF IN-PLANE SHEAR STRENGTH AND STIFFNESS OF SANDWICH COMPOSITES IN FOUR-POINT BENDING

Both out-of-plane shear strength and stiffness are determined from four-point bending experiments. However, even though datasheets are provided by the manufacturer, there are no data provided in the datasheets on the out-of-plane shear strength and out-of-plane stiffness. We convert the in-plane shear strength and in-plane-shear stiffness of the end-grain balsa core to the corresponding out-of-plane properties for analysis³⁶. We carried out the DIC strain measurement to convert the out-of-plane shear strain to the in-plane shear strain and then transferred the out-of-plane shear strength and modulus to in-plane shear strength and modulus to compare with the 3D-printed lattice core and the end-grain balsa core sandwich composites. All the computation is following the FSDT beam theory.

The specimen dimensions and in-plane and out-of-plane directions are shown in Fig. 7.

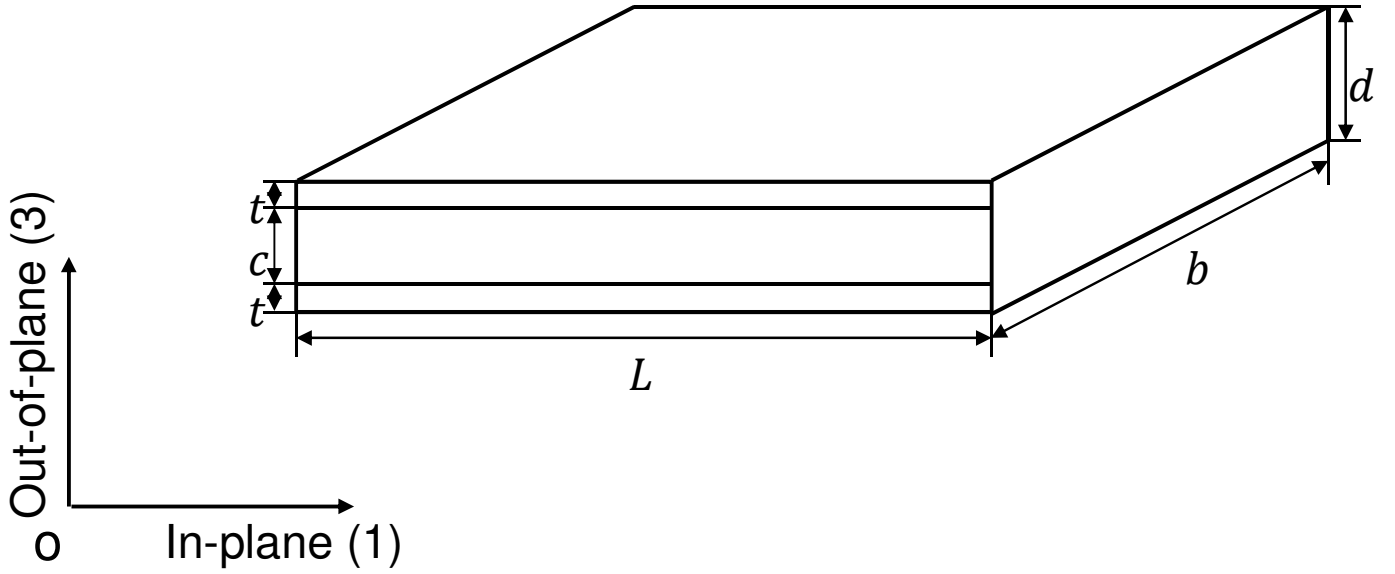


Figure 7: Specimen dimensions and in-plane and out-of-plane directions of the sandwich composites.

The out-of-plane shear strength and stiffness can be determined by the ASTM C393 standard. The in-plane shear strength is calculated following the ASTM D2344³⁷ using

$$\tau_{in} = 0.75 \frac{P_2}{bd} \quad (1)$$

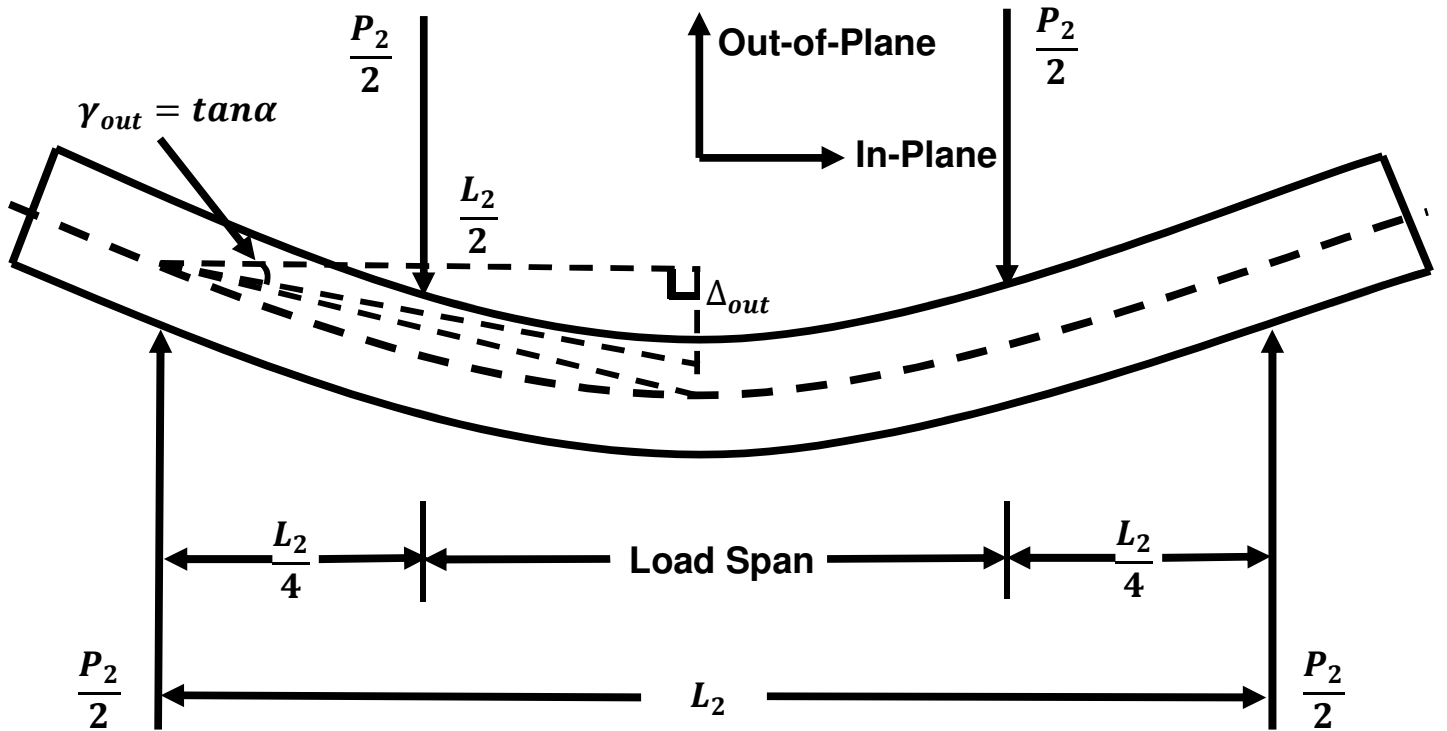


Figure 8: Schematic diagram of the sandwich composites under the four-point bending test.

Next, the out-of-plane shear strain is calculated by

$$\gamma_{out} = \tan\alpha = \frac{-\Delta_{out}}{0.5 \cdot L_2} = \frac{-2\Delta_{out}}{L_2} \quad (2)$$

where Δ_{out} is the out-of-plane shear deflection shown in Fig. 8. In four-point bending, the effective support span which carries the shear loads is the distance between the loading span and the support span (in our case, it is $0.5L_2$). Here, the out-of-plane engineering shear strain is considered to be approximately the ratio of out-of-plane shear deflection to half of the effective support span. The out-of-plane shear deflection ($\Delta_{out} = \frac{P_2L_2}{8U}$) is calculated from the total deflection (the total deflection: Δ_2) following the ASTM C393 standard.

$$\Delta_2 = \frac{11P_2L_2^3}{768R} + \frac{P_2L_2}{8U} \quad (3)$$

Here, the shear rigidity of the sandwich composites is $U = G_{out}(d+c)^2b/4c$; the second term in eq. (3) is the out-of-plane shear deflection. Plugging the shear rigidity term into the out-of-plane shear deflection (Δ_{out} in eq. (2)), we have

$$\Delta_{out} = \frac{P_2L_2c}{2G_{out}(d+c)^2b} \quad (4)$$

Next, substituting eq. (4) into eq. (2), the out-of-plane shear strain is determined as

$$\gamma_{out} = \frac{P_2c}{G_{out}(d+c)^2b} \quad (5)$$

Here, from the DIC results, the ratio of the in-plane shear strain to the out-of-plane shear strain is constant ($\nu = 0.35$), it is used to calculate the in-plane shear strain.

$$\nu = -\frac{\gamma_{in}}{\gamma_{out}} \quad (6)$$

Substituting eq. (5) into eq. (6), the in-plane shear strain is

$$\gamma_{in} = \frac{-P_2c\nu}{G_{out}(d+c)^2b} \quad (7)$$

Finally, the in-plane shear stiffness is determined as

$$G_{in} = \frac{\tau_{in}}{\gamma_{in}} = \frac{3(d+c)^2}{4\nu dc} G_{out} \quad (8)$$

4. RESULTS AND DISCUSSION

The 3D printing filaments were selected through the three-point bending tests. And the details on bending and shear properties of the PLA core and conventional core sandwich composites are described in this section.

4.1 The effects of infill density, deposited layer orientation, and filament type on the flexural properties of 3D-printed lattice beams

Prior to shear properties of 3D-printed core sandwich composite investigations, a proper 3D printing filament and manufacture setting should be chosen. So, the 3D-printed lattice beams were investigated by three-point bending tests. The detailed results are summarized in the supplementary file. PLA materials stand out compared with the rest of the 3D-printed beams due to their high mechanical performance and cost-effectiveness. A systematic comparison between 3D-printed and conventional core materials is shown in Fig. 9.

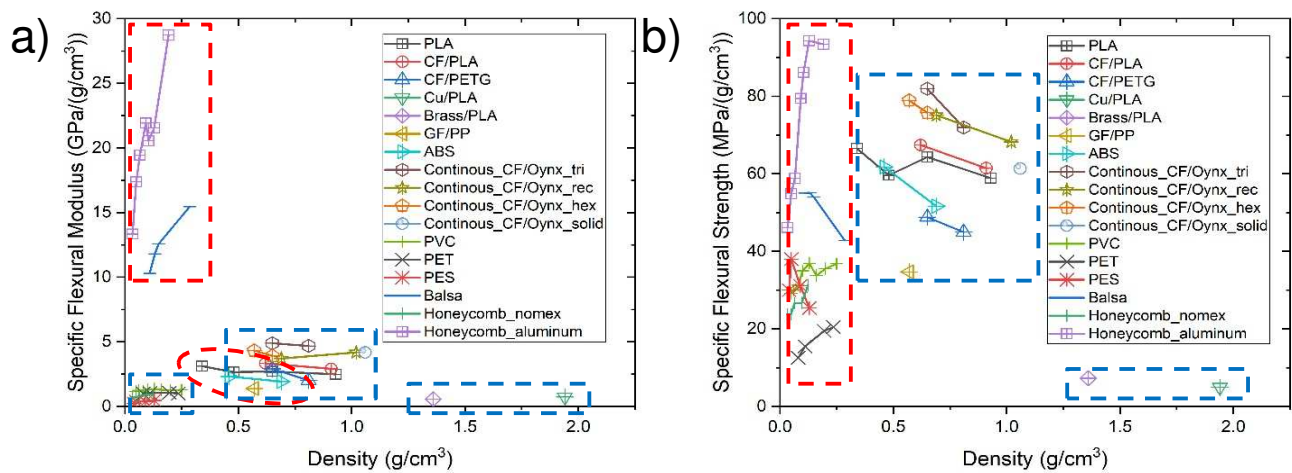


Figure 9: Specific flexural properties versus density of 3D-printed polymer beams, foam, and honeycomb structures: a) specific flexural modulus versus density; b) specific flexural strength versus density³⁸⁻⁴². (Note: the red dashed line zone is indicating the conventional material, the blue dashed line zone is indicating the 3D-printed material.)

A detailed comparison of the specific flexural strength and modulus between the 3D-printed polymer beams, foam, and honeycomb structures is shown in Fig. 9. Before stepping into the shear properties investigation, a proper thermoplastic polymer for 3D printing process should be chosen by comparing the specific bending stiffness and strength of the conventional polymer core (like PVC foam, PET foam, etc.) and the 3D-printed core. Although the continuous carbon fiber onyx matrix 3D-printed beams possess a better specific bending stiffness and strength, the cost is much higher than PLA which is not cost-effective. Chopped fiber/thermoplastic 3D-printed beams possess a lower bending stiffness and strength than 3D-printed pure thermoplastic beams. Although the chopped carbon fiber/PLA possesses a better specific bending stiffness and strength than all the other 3D-printed thermoplastic polymer beams, whether the chopped carbon fiber is cost-effective for the core materials remains uncertain. So, the PLA material stands out among all the rest of 3D printing materials. As for the conventional core materials, the aluminum honeycomb possesses the highest specific bending stiffness and strength. However, the metal materials are not chemically stable compared to polymer cores. So, the balsa is selected for the conventional core materials for benchmark purposes. The PVC foam is also selected for benchmark purposes since it is one of the most widely used core materials in the sandwich structure.

4.2 The effect of resin uptake on the shear strength and stiffness of compression-molded sandwich composites

The in-plane shear and out-of-plane shear of sandwich composites were investigated by three-point bending and four-point bending tests. Whether the 3D-printed PLA beam is suitable for engineering application and how the resin uptake affects the sandwich structure was illustrated in this section.

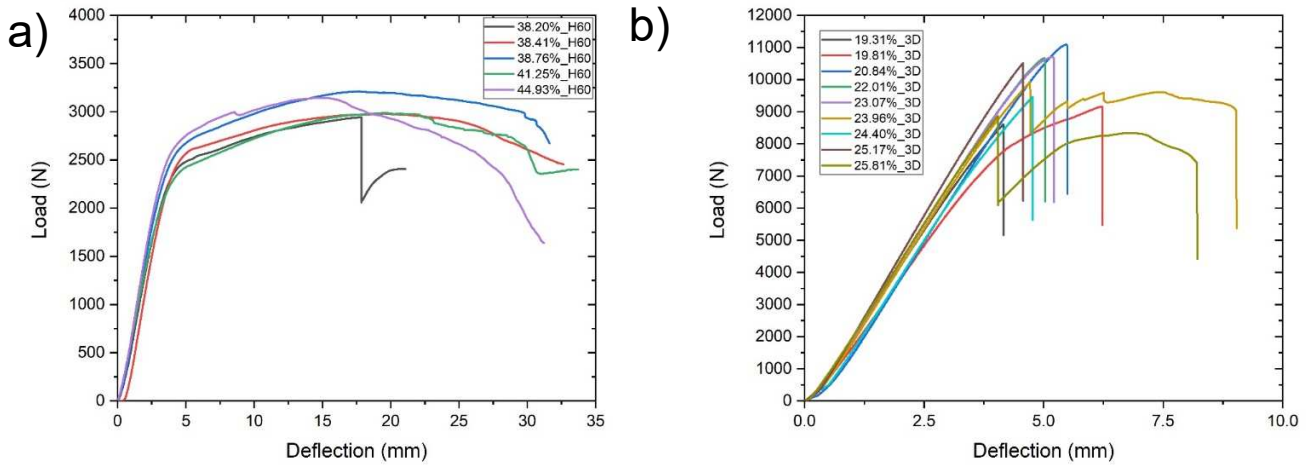


Figure 10: Load vs deflection curve for sandwich composites with four types of core and multiple levels (H60 core: 38%~44% and 3D-printed core: 19~25%) of resin uptake sandwich composites under four point bending loads: a) H60 PVC core; b) PLA core.

| Core Material | w_R (%) | L (mm) | c (mm) | b (mm) | d (mm) |
|------------------------------|--------------|-------------|-------------|-------------|-------------|
| H60_PVC | 38.41 | 101.6 | 12.7 | 48.12 | 16.17 |
| | 41.25 | 101.6 | 12.7 | 48.01 | 16.61 |
| | 44.93 | 101.6 | 12.7 | 49.09 | 17.32 |
| 15%/3D-tri infill_ PLA | 19.31 | 101.6 | 12.7 | 52.19 | 17.92 |
| | 19.81 | 101.6 | 12.7 | 51.88 | 17.98 |
| | 20.84 | 101.6 | 12.7 | 51.76 | 17.12 |
| | 22.01 | 101.6 | 12.7 | 51.58 | 17.17 |
| | 23.07 | 101.6 | 12.7 | 50.85 | 16.27 |
| | 23.97 | 101.6 | 12.7 | 51.98 | 17.72 |
| | 24.40 | 101.6 | 12.7 | 51.51 | 17.42 |
| Balsasud _End Grain Balsa | 25.17 | 101.6 | 12.7 | 51.96 | 17.59 |
| | 25.81 | 101.6 | 12.7 | 51.88 | 17.97 |
| | 70.23 | — | 12.7 | 50.80 | 16.70 |
| | 58.87 | — | 12.7 | 50.80 | 16.70 |
| | 51.52 | — | 12.7 | 50.80 | 16.70 |

Table 1: A summary of resin uptake (w_R), span length, and specimen geometries of compression-molded sandwich composites under four point bending loads.

The load versus deflection curves for sandwich composites under three-point bending and four-point bending are shown in Fig. 10. Based on the peak bending loads of sandwich composites from Fig. 10, the 3D-printed lattice core is more sensitive to the level of resin uptake due to lower flexibility than the H60 PVC foam core. This phenomenon is even apparent under the three-point bending tests. When the resin uptake increases, the peak load of H60 PVC foam core sandwich composites increases under four-point bending loads. As for the 3D-printed lattice core sandwich composites, when the resin uptake increases, the peak load increases and then decreases. This indicates that the 3D-printed core sandwich composites need to modify the resin uptake at an adequate level to get the best bending load capacity.

A summary is provided in Table 1 on the resin uptake, span length, and specimen geometries of the compression-molded sandwich composites. The span to depth ratios for four-point bending is 8:1. Such a span-to-depth ratio in four-point bending is chosen to maximize the shear loads in the core of sandwich composites. Since the out-of-plane shear strength and stiffness are calculated under two loading conditions (three-point bending and four-point bending), two specimens with the resin uptake difference within 1% are considered identical. Here, the core thickness used is 12.7 mm. Therefore, the width and depth are an average value of two specimens within 1% of resin uptake difference. Based on the UD970 glass fabric and BALSASUD datasheets^{39,49}, the resin uptake of the balsa core/UD970 glass skin sandwich composites are listed in Table 1. The resin uptake in the balsa core sandwich composites is identical to that of the balsa and PVC foam core sandwich composites. The resin uptake of the balsa core sandwich composites is for benchmark purposes.

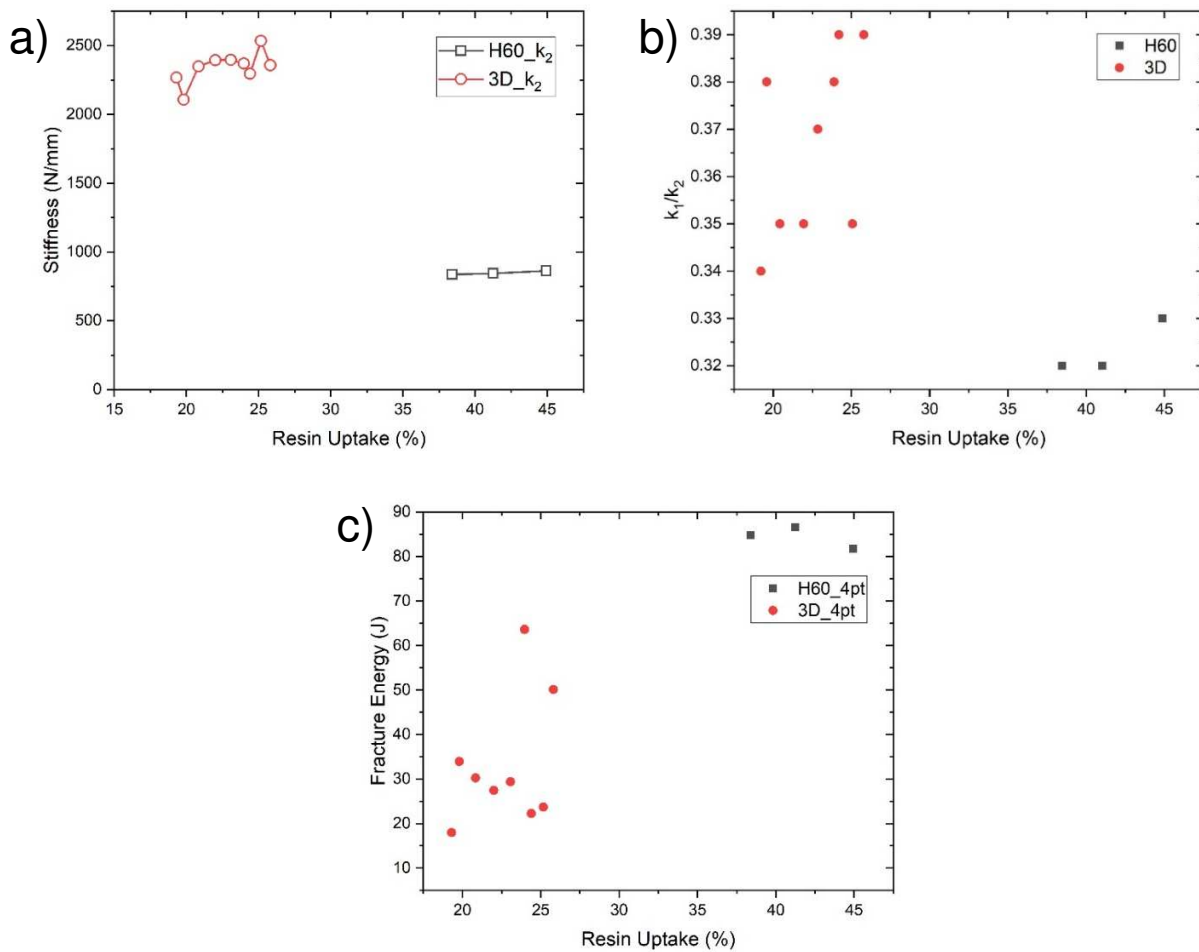


Figure 11: Scatter plot of various properties of 3D-printed core and H60 PVC foam core sandwich composites a) stiffness versus resin uptake; b) three-point bending to four-point bending stiffness ratio versus resin uptake; c) fracture toughness versus resin uptake. (Note: subscript 1 indicates the specimen conditions under the three-point bending, subscript 2 shows the specimen conditions under the four-point bending).

The scatter plots of stiffness, stiffness ratio, and fracture toughness versus resin uptake of the sandwich composites are shown in Fig. 11. In Fig. 11a, for the PLA core sandwich composites, four-point bending stiffness increase when the resin uptake increases. However, the stiffness of H60 PVC foam core sandwich composites remains relatively constant for varying levels of resin uptake. Based on the sandwich beam theory, the stiffness of resin is not compatible with the skin stiffness, and the effect of resin uptake can be neglected. So this theory is not appropriate for evaluating the PLA core sandwich composites. From Fig. 11b, the ratio of

three-point bending and four-point bending stiffness increased with respect to an increased resin uptake of the 3D-printed core sandwich composites. This indicates that a better skin-core bonding quality can be more beneficial to the bending than shear strength and stiffness in the 3D-printed core sandwich composites due to the different span lengths of bending tests. Because bending and shear stiffness keeps relatively constant for H60 PVC foam core composite, the ratio of three-point bending and four-point bending stiffness is also stable. Based on Fig. 11c, there are no direct correlations between the fracture toughness and the level of resin uptake. Because the resin uptake is not the only factor that drives the fracture toughness, the consistency of core flexibility, stiffness, and fracture initiation mechanism also influence the fracture toughness.

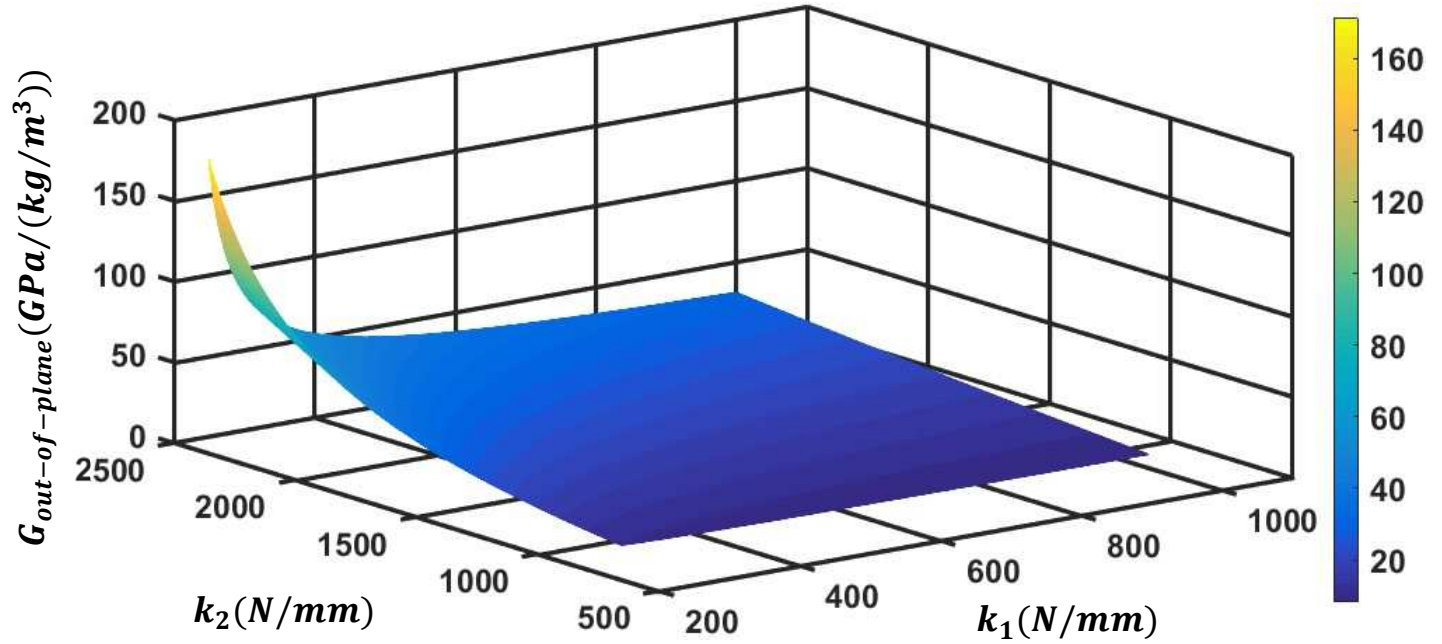


Figure 12: 3D contour plot of out-of-plane shear stiffness versus three-point bending and four-point bending stiffness for compression-molded sandwich composites.

3D contour plot of out-of-plane shear stiffness versus three-point bending (k_1) and four-point bending (k_2) stiffness of compression-molded sandwich composites is shown in Fig. 12. The span length ratio (L_1/L_2) was set as 2, and specimen dimensions were assumed as $12.7 \times 50.8 \times 254$ mm with 2 mm skin thickness. From Fig. 12, when the three-point bending stiffness keeps constant, a higher four-point bending stiffness leads to a higher out-of-plane shear stiffness. When the four-point bending stiffness keeps constant, a higher three-point bending stiffness leads to a lower out-of-plane shear stiffness. In our case, when considering the PLA core sandwich composites, the value of k_1/k_2 keeps increasing with the increase of resin uptake. From Fig. 12, higher values of k_1/k_2 leads to lower values of out-of-plane shear stiffness. However, this does not indicate the out-of-plane shear stiffness linearly decreases versus resin uptake, because k_1 is also increasing versus resin uptake. How the out-of-plane shear stiffness of the PLA core sandwich composites varies needs further investigation. The numerical values of peak force, displacement at peak force, stiffness, stiffness ratio, and fracture toughness are summarized in Table 2.

| Core Material | P_{max} (N) | S_{max} (mm) | k_2 (N/mm) | k_1/k_2 (-) | G_f (J) |
|---------------|------------------|-------------------|-----------------|------------------|--------------|
| H60_PVC | 2979.17 | 19.58 | 836.13 | 0.32 | 84.79 |
| | 2987.36 | 19.52 | 843.87 | 0.32 | 86.63 |
| | 3143.79 | 15.14 | 863.26 | 0.33 | 81.73 |

| | | | | | |
|---------------------------|----------|-------|---------|------|-------|
| 15%/3D-tri infill_ PLA | 8615.95 | 15.14 | 2266.44 | 0.34 | 17.97 |
| | 9159.36 | 6.22 | 2106.77 | 0.38 | 33.96 |
| | 11083.15 | 5.47 | 2348.70 | 0.35 | 30.27 |
| | 10667.97 | 5.02 | 2393.88 | 0.35 | 27.44 |
| | 10701.05 | 5.19 | 2396.33 | 0.37 | 29.40 |
| | 9920.35 | 4.71 | 2369.83 | 0.38 | 63.60 |
| | 9459.38 | 4.77 | 2294.60 | 0.39 | 22.25 |
| | 10512.55 | 4.71 | 2534.64 | 0.35 | 23.70 |
| | 8865.42 | 4.04 | 2357.97 | 0.39 | 50.14 |

Table 2: A summary of peak force (P_{max}), displacement at peak force (S_{max}), stiffness (k_2), stiffness ratio (k_1/k_2), and fracture toughness ($G_{f,2}$) of compression-molded sandwich composites under four-point bending.

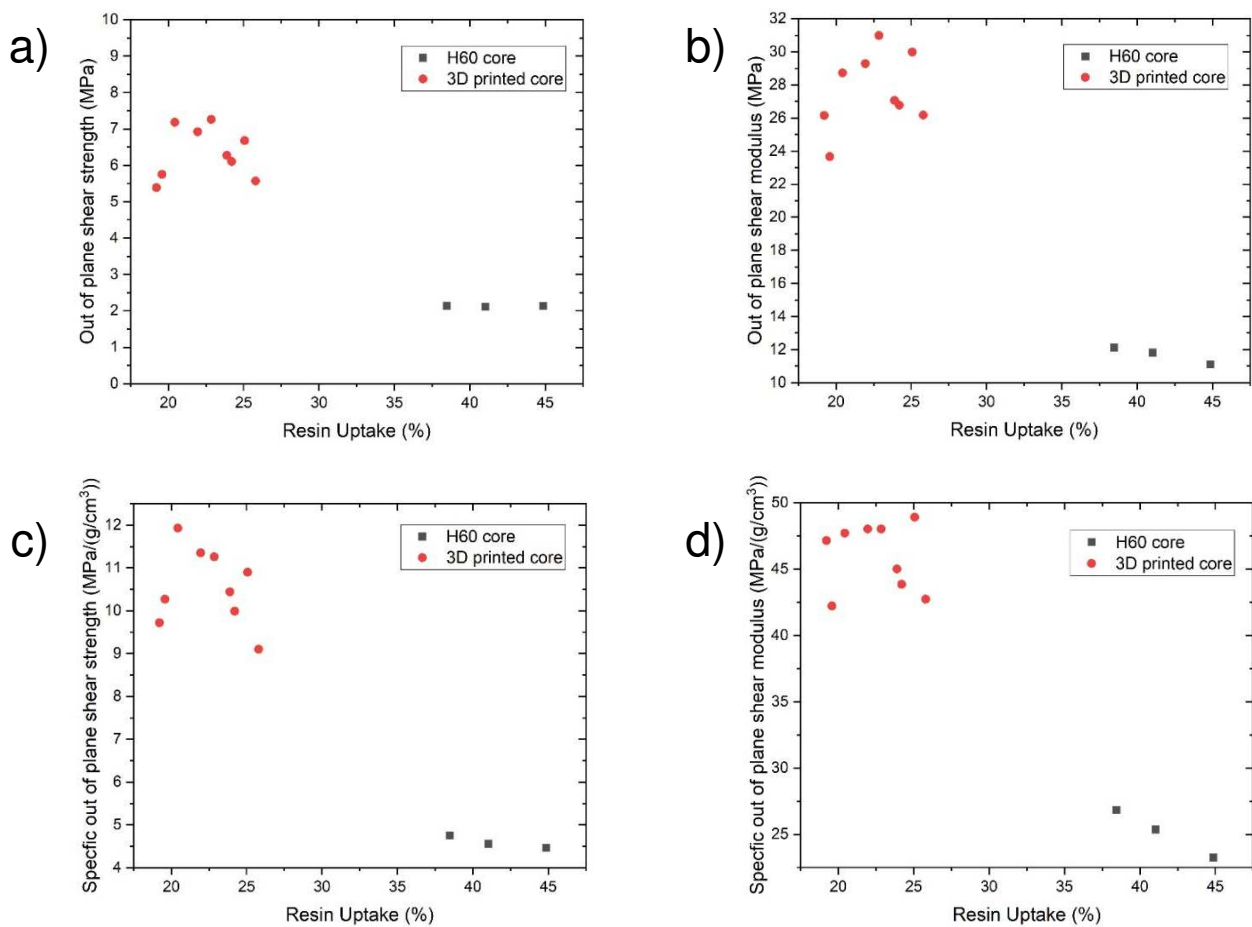


Figure 13: Scatter plots of out-of-plane shear strength and stiffness versus resin uptake of compression-molded sandwich composites: a) out-of-plane shear strength; b) out-of-plane shear stiffness; c) specific out-of-plane shear strength; d) specific out-of-plane shear stiffness.

Scatter plots of out-of-plane shear strength and stiffness versus resin uptake of PLA core, and H60 PVC foam core sandwich composites are shown in Fig. 13. The optimized resin uptake regime of PLA core sandwich composites is from 20.43% to 22.86%. In the PLA core sandwich composites, the specific out-of-plane shear strength and stiffness increase versus increased resin uptake due to a better skin-core bonding quality. The specific out-of-plane shear strength and stiffness decrease versus increased resin uptake. Compared with the H60 PVC foam core sandwich composites, the out-of-plane shear strength and stiffness of 3D-printed core sandwich composites are around 2~3 times higher, and the specific out-of-plane shear strength and stiffness are

2~3 and ~2 times higher, respectively.

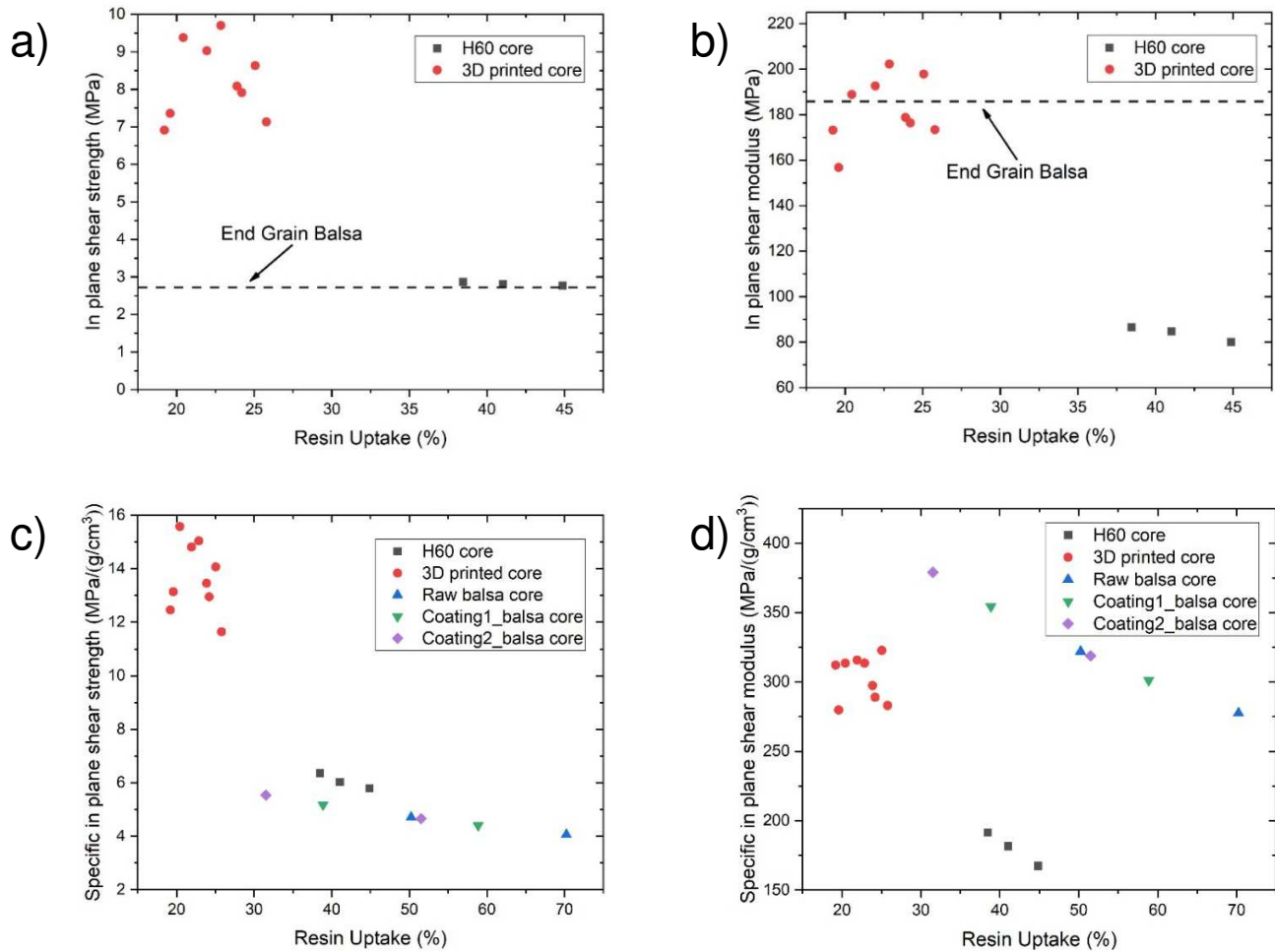


Figure 14: In-plane shear strength and stiffness versus resin uptake of compression-molded sandwich composites: a) in-plane shear strength; b) in-plane shear stiffness; c) specific in-plane shear strength; d) specific in-plane shear stiffness.

The measured in-plane shear strength and stiffness are plotted versus the resin uptake in the sandwich specimens with 3D-printed core, H60 PVC foam core, and balsa core are shown in Fig. 14. Based on the sandwich beam theory and BALSASUD datasheets, the in-plane shear strength, and stiffness of balsa core sandwich composites are considered as 2.72 and 186 MPa with 0.152 g/cm³ nominal core density. These numerical values were used in multiple wind turbine blade structure performance simulation⁵⁰⁻⁵³. Based on the ASTM standards and 2D-DIC results, the in-plane shear stiffness was determined from out-of-plane shear strength and stiffness. The 3D-printed core sandwich composites have 2~3 times higher in-plane shear strength and similar in-plane shear stiffness than balsa core sandwich composites. The 3D-printed core sandwich composites also possess 3~3.5 times higher specific in-plane shear strength than balsa core sandwich composites. The specific in-plane shear stiffness of 3D-printed and raw balsa core sandwich composites are similar. The UV light curing epoxy-based agent coated balsa core sandwich composites possess 8.19% and 15.16% higher specific in-plane shear stiffness than 3D-printed core sandwich composites within all resin uptake regimes, and 9.81% and 17.44% higher within an optimized resin uptake regime. Generally speaking, the 3D-printed core stands out among conventional core materials in shear strength and specific shear strength and stiffness. The 3D-printed core possesses slightly lower specific in-plane shear stiffness than the UV light-curing epoxy-based agent-coated balsa core. This can be enhanced by modifying the skin/core interphase appropriately. Compared with raw balsa core and PLA core, these two materials possess similar in-plane shear

strength and stiffness. But the 3D-printed core could be more cost-effective because this core could save resin during manufacture compared with the balsa core. A summary of in-plane and out-of-plane shear of 3D-printed, H60 PVC foam, and balsa core sandwich composites are listed in Table 3 and Table 4.

| Core Material | ρ_{all} (g/cm^3) | ν (-) | τ_{out} (MPa) | G_{out} (MPa) | τ_{out}/ρ_{all} (GPa / (kg/m^3)) | G_{out}/ρ_{all} (GPa / (kg/m^3)) | τ_{in} (MPa) | G_{in} (MPa) | τ_{in}/ρ_{all} (GPa / (kg/m^3)) | G_{in}/ρ_{all} (GPa / (kg/m^3)) |
|--------------------------------|---------------------------|-----------|--------------------|-----------------|--|---|-------------------|----------------|---|--|
| H60_PVC | 0.45 | 0.32 | 2.14 | 12.11 | 4.75 | 26.84 | 2.87 | 86.43 | 6.36 | 191.46 |
| | 0.47 | 0.32 | 2.12 | 11.82 | 4.56 | 25.36 | 2.81 | 84.59 | 6.03 | 181.57 |
| | 0.48 | 0.32 | 2.13 | 11.11 | 4.46 | 23.25 | 2.77 | 80.04 | 5.80 | 167.42 |
| | 0.55 | 0.35 | 5.39 | 26.15 | 9.72 | 47.16 | 6.91 | 173.14 | 12.46 | 312.24 |
| 15%/3D-tetra infill_ PLA | 0.56 | 0.35 | 5.75 | 23.66 | 10.27 | 42.22 | 7.36 | 156.76 | 13.14 | 279.72 |
| | 0.60 | 0.35 | 7.18 | 28.73 | 11.93 | 47.72 | 9.38 | 188.84 | 15.58 | 313.64 |
| | 0.61 | 0.35 | 6.92 | 29.29 | 11.35 | 48.02 | 9.03 | 192.61 | 14.81 | 315.80 |
| | 0.65 | 0.35 | 7.26 | 30.98 | 11.26 | 48.03 | 9.70 | 202.24 | 15.04 | 313.50 |
| | 0.60 | 0.35 | 6.27 | 27.06 | 10.44 | 45.01 | 8.08 | 178.81 | 13.46 | 297.42 |
| | 0.61 | 0.35 | 6.10 | 26.77 | 9.99 | 43.85 | 7.91 | 176.40 | 12.95 | 289.00 |
| | 0.61 | 0.35 | 6.68 | 29.98 | 10.90 | 48.91 | 8.63 | 197.88 | 14.07 | 322.81 |
| | 0.61 | 0.35 | 5.57 | 26.17 | 9.10 | 42.73 | 7.13 | 173.39 | 11.64 | 283.03 |

Table 3: In-plane and out-of-plane shear strength and stiffness of 3D-printed and H60 PVC foam core sandwich composites.

| Core Material | $w_{R,min}$ (%) | $w_{R,max}$ (%) | $\rho_{all,min}$ (g/cm^3) | $\rho_{all,max}$ (g/cm^3) | τ_{in} (MPa) | G_{in} (MPa) | $\tau_{in,min}/\rho_{all,min}$ (GPa / (kg/m^3)) | $\tau_{in,max}/\rho_{all,max}$ (GPa / (kg/m^3)) | $G_{in,min}/\rho_{all,min}$ (GPa / (kg/m^3)) | $G_{in,max}/\rho_{all,max}$ (GPa / (kg/m^3)) |
|----------------|-----------------|-----------------|-------------------------------|-------------------------------|-------------------|----------------|---|---|--|--|
| Raw balsa | 50.23 | 70.23 | 0.58 | 0.67 | | | 4.06 | 4.71 | 277.50 | 322.11 |
| Coating1_balsa | 38.87 | 58.87 | 0.52 | 0.62 | 2.72 | 186 | 4.40 | 5.18 | 301.19 | 354.47 |
| Coating2_balsa | 31.52 | 51.52 | 0.49 | 0.58 | | | 4.66 | 5.54 | 318.80 | 379.11 |

Table 4: Out-of-plane shear strength and stiffness of balsa core sandwich composites.

4.3 Surface strain distribution of compression-molded sandwich composites by 2D-DIC technique

The surface strain distribution of two types of sandwich composites is shown in Fig. 15.

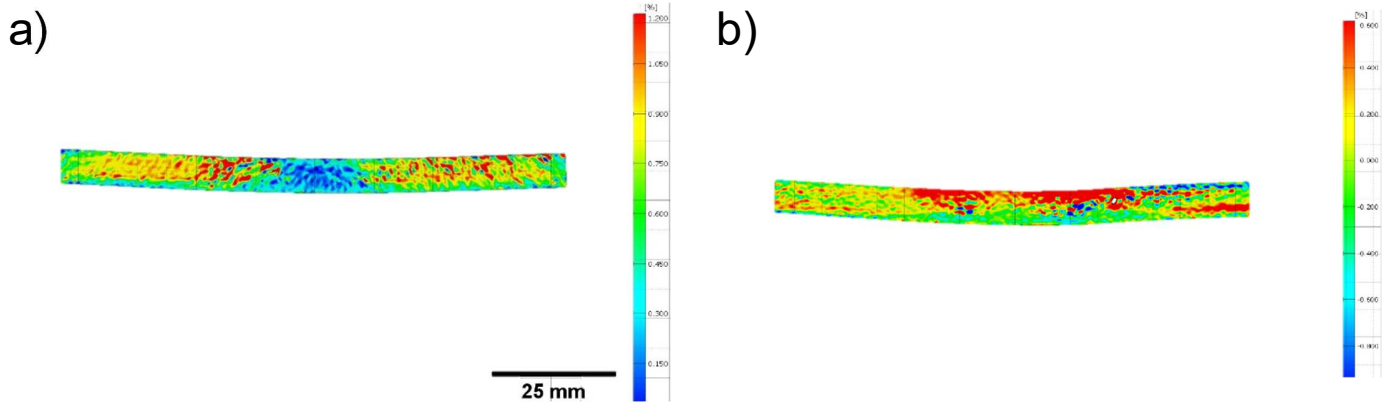


Figure 15: First order principal strain distribution of the PLA lattice core sandwich composites: a) the sandwich composite of 19.31% resin uptake under four-point bending load with 64s timeframe; b) the sandwich

composite of 23.97% resin uptake under four-point bending load with 97s timeframe.

To fully evaluate the structural integrity of the 3D-printed sandwich composites, the 2D-DIC technique was employed to further visualize the surface strain during the four-point bending tests. The surface strain distribution of two types of sandwich composites is shown in Fig. 15. From Fig. 15a, a lower resin uptake could lead to an uneven strain distribution in the core due to an insufficient amount of resin in the interphase. However, an adequate level of resin uptake could introduce a proper amount of resin to achieve a sufficient shear stress transfer from the skin to the core. Comparing Fig. 15a with 15b, the surface strain distributed between the loading span and loading nose when four-point bending loads are relatively low. When a high level of four-point bending loads is applied to the sandwich composite, the surface strain concentrates below the two indenter pins. Also, a certain amount of negative strain was captured at the right span and below the two indenter pins. This indicates that failure will most likely arise in these regions, which will be a skin-core debonding and core shearing failure mode. So, modification of the resin uptake in the PLA lattice core sandwich composites is crucial for structural integrity due to the skin/core debonding in the early stage of the structural loading.

4.4 Failure modes for the 3D-printed and H60 PVC foam core sandwich composites

Figure 16 shows the failure modes of PLA lattice core sandwich composites under multiple levels of resin uptake.

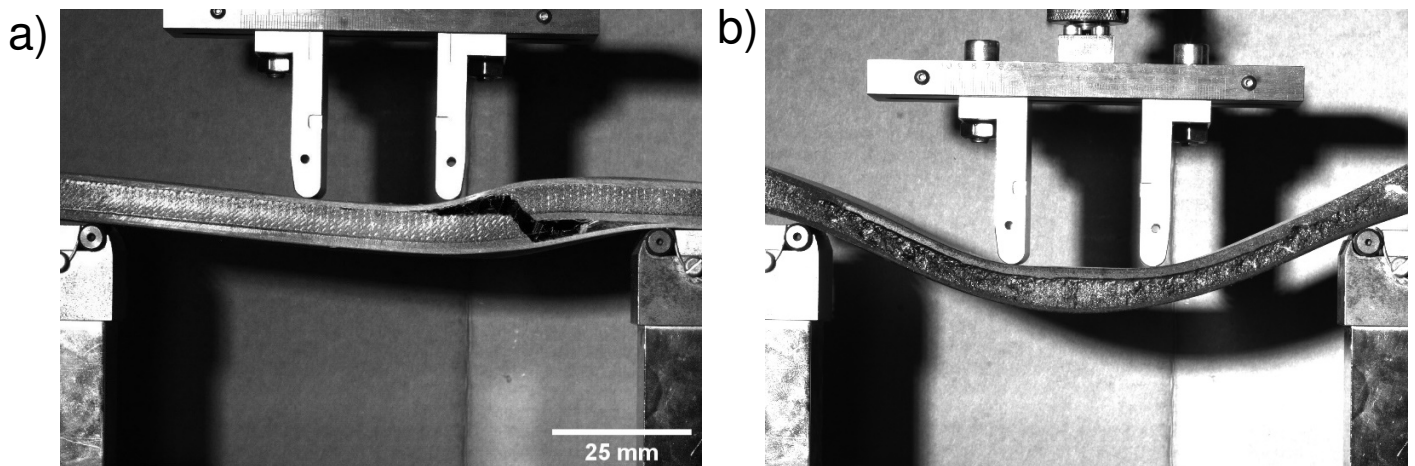


Figure 16: Failure modes of the PLA lattice and PVC foam core sandwich composites under four point bending tests: a) skin/core debonding and core shearing failure (PLA); b) skin/core debonding, core shearing, and core crushing failure (PVC foam).

In the four-point bending tests, all the PLA lattice core sandwich composites exhibited a skin/core debonding and core shearing failure, and all the H60 PVC foam core sandwich composites exhibited an extra core crushing failure. This phenomenon indicates that the PLA core has higher stiffness than the H60 PVC foam core. However, the PVC foam core can sustain a larger energy absorption due to better skin/core bonding. Most of the PLA lattice core sandwich composites exhibited a skin/core debonding and core shearing failure in the three-point bending tests. Most of the H60 PVC foam core sandwich composites exhibited local indentation failure²⁹. This indicates that in the H60 PVC foam core sandwich composites, the skin/core bonding quality is sufficiently high to carry and transfer the shear loads from the skin to the core. However, the 3D-printed core is much stiffer than the H60 PVC foam core, and the skin/core can be considered the most vulnerable region in the sandwich composites. In general, the PVC foam core should be stiff enough to carry the shear loads in the actual structure, and the skin/core interphase of the 3D-printed core sandwich composites should be enhanced to prevent structure catastrophic failure.

5. DISCUSSION ON MECHANICAL PROPERTIES OF FDM/CM MANUFACTURED SANDWICH

COMPOSITES

Although the 3D-printed core possesses higher in-plane, out-of-plane shear strength and similar in-plane, out-of-plane shear modulus compared with balsa core. It is still not clear whether it is possible to replace the skin material with a high-efficiency recyclable material (like thermoplastic matrix, etc.) with a compatible mechanical performance with conventional skin material. A detailed comparison between recyclable skin, PLA core and glass skin, balsa core is shown in Table 5.

| Reference | Core Material / t_c (mm) | Skin Material / t_s (mm) | Process | τ_ρ^{in} | τ_ρ^{out} | G_ρ^{in} | G_ρ^{out} | σ_ρ | D_ρ^b | k_ρ^b | U_ρ^b |
|---------------------------------|----------------------------|----------------------------|--------------------|--------------------------------------|-------------------|--|--|--|-----------------------------------|--------------------------------------|-------------------|
| – | PLA lattice truss/12.7 | GFRP /2 | FDM-CM | 601.8~714.9 (N/g) | 469.4~535.1 (N/g) | 507.8~579.2 (MPa/(g/cm ³)) | 42.73~48.91 (GPa/(Kg/m ³)) | 27.5~35.7 (N/g) | 1.15~1.23 (kN*m ² /kg) | 2.3~2.7 (kN/mm)/(g/cm ³) | 90.3~242.7 (J/Kg) |
| | | | | 49.4~82.2 (MPa/kg) | | | | 592.1~767.1 (MPa/kg) | 23.8~26.7 (kN*mm/g) | 20.3~24.2 (GPa/(g/cm ³)) | |
| | | | | 20.9~28.0 (MPa/(g/cm ³)) | | | | 206.4~296.6 (MPa/(g/cm ³)) | | | |
| Pirouzf ar et al. ⁴⁹ | PLA honeycomb/1~2 | GFRP /1 | FDM-WL-Adhesive | 1.4~2.9 (MPa/kg) | – | – | – | 70.4~145.6 (MPa/kg) | 125~450 (N*m ² /kg) | – | 26.4~28.5 (J/Kg) |
| Ridlwan et al. ⁵⁰ | PLA lattice truss /5~15 | GFRP /2~4 | FDM-VARTM-Adhesive | – | – | – | – | – | 46~48 (kN*mm/g) | – | – |
| Azzouz et al. ⁵¹ | PLA lattice truss /10 | Flax/PP /1 | FDM-VARTM-Adhesive | 533~830 (N/g) | – | – | – | 26~34 (N/g) | – | – | – |
| Monti et al. ⁵² | Balsa /15.9 | Recycled Flax/Elium /2 | VARTM | 6.7 (MPa/(g/cm ³)) | – | 600 (MPa/(g/cm ³)) | – | 240~320 (MPa/(g/cm ³)) | – | 800~1600 (N/mm)/(g/cm ³) | – |
| Awad et al. ⁵³ | Balsa/GFRP /12 | GFRP /3 | VARTM | 3.6 (MPa/(g/cm ³)) | – | – | – | 198.2 (MPa/(g/cm ³)) | – | 14.4 (GPa/(g/cm ³)) | – |

Table 5: A comparison of flexural and shear properties between 3D-printed PLA and balsa core sandwich composites. (Notice: 1. WL: wet layup process, Flax: natural flax fabrics, PP: polypropylene, Elium: liquid thermoplastic resin; 2. t_c : the thickness of the core, t_s : the thickness of skin, τ_ρ^{in} : specific in-plane shear stress or specific peak in-plane shear load, τ_ρ^{out} : specific out-of-plane plane shear stress, G_ρ^{in} : specific in-plane shear modulus, G_ρ^{out} : specific out-of-plane plane shear modulus, σ_ρ : specific flexural strength or specific peak bending load, D_ρ^b : specific flexural rigidity, k_ρ^b : specific flexural stiffness, U_ρ^b : specific energy absorption under bending load.)

Compared with Pirouzf ar et al.⁴⁹, a sufficient thickness of the sandwich structure plays a significant role in achieving good bending and shear strength and stiffness. Based on Ridlwan et al.⁵⁰ investigation, applying glass skin on both the top/bottom and width side of the core can greatly enhance the flexural rigidity of the sandwich composite. Compared with Azzouz et al.⁵¹ results, flax fabric with PP thermoplastic matrix skin possesses a similar specific peak bending and shear load to glass fabric and epoxy resin matrix. This finding indicates that using the natural fiber and thermoplastic polymers in the sandwich composites not only maintains similar mechanical properties to the glass fiber/thermoset matrix skin sandwich structure, which is safe to use in many applications but also the sandwich composite is fully recyclable and can greatly reduce the chance for environmental pollution. Based on Monti et al.⁵² findings, using a recycled flax fiber composite skin can still reach good structure stability, but the shear and bending strength keep decreasing based on the time and method of recycling. Compared to Monti et al.⁵² and Awad et al.⁵³ results, a 3D-printed core can give a higher shear

strength than a balsa core, which is consistent with Figs. 13 and 14.

CM process plays a critical role in modifying the bending and shear properties of the 3D-printed core sandwich composites by changing the resin amount in the skin/core interphase. Because the chemical bonding between epoxy resin and PLA is different from the conventional core material. Modifying the amount of resin on the skin/core interphase can be the first step in strengthening the 3D-printed core sandwich composites. Furthermore, there is a great potential for further improving mechanical performance by considering modifying materials and maintaining adequate resin on the skin/core interphase of the 3D-printed core sandwich composite.

6. CONCLUSION

3D-printed PLA core sandwich composites were fabricated by the FDM/CM approach. Compared with VARTM or VARTM/adhesive bonding process, the advantage of the FDM approach is that it can produce an improved core infill pattern to strengthen the core stiffness and strength and increase the homogeneity of the core structure. Compared with VARTM/FDM/adhesive bonding process, the CM approach can modify the resin uptake in the skin and skin/core interphase region. Based on our investigation, modifying the resin uptake in the skin and skin/core interphase cannot greatly affect the bending or shear stiffness of the balsa and PVC foam sandwich composites, which are mainly affected by core density and the amount of fibers in the skin. However, for 3D-printed core sandwich composites, the amount of resin absorbed in the skin/core interphase plays a significant role in influencing the bending and shear properties of 3D-printed core sandwich composites due to a different chemical bonding mechanism. The CM process can easily modify the resin uptake by varying the level of compression applied to the sandwich composite, and this process is more suitable than conventional manufacturing routines (VARTM, adhesive bonding, etc.) when a 3D-printed thermoplastic core is used in the sandwich structure.

The out-of-plane and in-plane shear strength and stiffness of two types of core sandwich composites were investigated by three-point bending and four-point bending tests and derived through the FSDT theory. In the 3D-printed core sandwich composites, based on the information on specific out-of-plane shear strength and stiffness, the optimized resin uptake regime of PLA core sandwich composites is from 20.43% to 22.86%. Insufficient resin in the skin/core interphase cannot carry the shear load from the skin to the core. Based on the information of 2D-DIC, an insufficient amount of resin in the skin/core interphase could lead to an uneven strain distribution in the core. A resin-rich zone on the skin/core interphase will not be beneficial to the sandwich structure due to low ductility in this region.

3D-printed PLA core stands out among the conventional PVC core materials and is similar to conventional balsa core materials in terms of shear and specific shear strength and stiffness. The use of thermoplastic resin/polymer] can greatly reduce the recycling cost and environmental pollution. Although balsa is a naturally grown and sustainable material, the recycling efficiency is low after the resin is impregnated inside of balsa. Since resin uptake in the skin/core interphase region of the 3D-printed PLA core sandwich composites plays a critical role in mechanical performance. A suitable strategy for skin/core interphase enhancement warrants further study. Also the level of degradation of recycled PLA mechanical performance compared to virgin materials should be examined. As a result, this work presents some new and important findings that support the greater use of additive manufacturing of core materials for use in sandwich composites in many applications such as wind turbine blades and aerospace structures by providing benefits in terms of manufacturability and recyclability.

ACKNOWLEDGMENTS

We acknowledge the support of National Science Foundation (NSF) WindStar I/UCRC Center (IIP-1362033 and IIP-1916776), DoE under DE-NA0003962 and DE-NA-0003525, and also NSF CMMI-1661246, CMMI-1636306, and CMMI-1726435. Lu also acknowledges the support of the Louis A. Beecherl Jr. Chair.

REFERENCES

1. Schuler N, Casalis A, Debomy S, et al. What a Waste : A Global Review of Solid Waste Management. *World bank group*. 2012;(7). Accessed September 24, 2022. <https://openknowledge.worldbank.org/handle/10986/17388>
2. Rani M, Choudhary P, Krishnan V, Zafar S. A review on recycling and reuse methods for carbon fiber/glass fiber composites waste from wind turbine blades. *Compos B Eng*. 2021;215:108768. doi:10.1016/J.COMPOSITESB.2021.108768
3. Reis JP, Moura M de, Samborski S. Thermoplastic Composites and Their Promising Applications in Joining and Repair Composites Structures: A Review. *Materials 2020, Vol 13, Page 5832*. 2020;13(24):5832. doi:10.3390/MA13245832
4. Xu M xin, Ji H wen, Wu Y chang, et al. The pyrolysis of end-of-life wind turbine blades under different atmospheres and their effects on the recovered glass fibers. *Compos B Eng*. 2023;251:110493. doi:10.1016/J.COMPOSITESB.2022.110493
5. Wang X, Jiang M, Zhou Z, Gou J, Hui D. 3D printing of polymer matrix composites: A review and prospective. *Compos B Eng*. 2017;110:442-458. doi:10.1016/j.compositesb.2016.11.034
6. Zhuo P, Li S, Ashcroft IA, Jones AI. Material extrusion additive manufacturing of continuous fibre reinforced polymer matrix composites: A review and outlook. *Compos B Eng*. 2021;224:109143. doi:10.1016/J.COMPOSITESB.2021.109143
7. Blok LG, Longana ML, Yu H, Woods BKS. An investigation into 3D printing of fibre reinforced thermoplastic composites. *Addit Manuf*. 2018;22:176-186. doi:10.1016/J.ADDMA.2018.04.039
8. Matsuzaki R, Ueda M, Namiki M, et al. Three-dimensional printing of continuous-fiber composites by in-nozzle impregnation. *Scientific Reports 2016 6:1*. 2016;6(1):1-7. doi:10.1038/srep23058
9. Cao D, Malakooti S, Kulkarni VN, Ren Y, Lu H. Nanoindentation measurement of core–skin interphase viscoelastic properties in a sandwich glass composite. *Mech Time Depend Mater*. Published online 2020. doi:10.1007/s11043-020-09448-y
10. Wang X, Xu T, Andrade MJ De, et al. The Interfacial Shear Strength of Carbon Nanotube Sheet Modified Carbon Fiber Composites. In: *Challenges in Mechanics of Time-Dependent Materials*. Vol 2. Conference Proceedings of the Society for Experimental Mechanics Series; 2021. doi:10.1007/978-3-030-59542-5_4
11. Fatima NS, Dhaliwal GS, Newaz G. Influence of interfacial adhesive on impact and post-impact behaviors of CFRP/end-grain balsawood sandwich composites. *Compos B Eng*. 2021;212:108718. doi:10.1016/J.COMPOSITESB.2021.108718
12. Wang B, Luo B, Jiang R, et al. Double-layer woven lattice truss sandwich composite for multifunctional application: Design, manufacture and characterization. *Compos B Eng*. 2022;241:110026. doi:10.1016/J.COMPOSITESB.2022.110026
13. Qi C, Jiang F, Yang S. Advanced honeycomb designs for improving mechanical properties: A review. *Compos B Eng*. 2021;227:109393. doi:10.1016/J.COMPOSITESB.2021.109393
14. Sun M, Wowk D, Mechefske C, Alexander E, Kim IY. Surface and honeycomb core damage in adhesively bonded aluminum sandwich panels subjected to low-velocity impact. *Compos B Eng*. 2022;230:109506. doi:10.1016/J.COMPOSITESB.2021.109506

15. Proença M, Garrido M, Correia JR, Gomes MG. Fire resistance behaviour of GFRP-polyurethane composite sandwich panels for building floors. *Compos B Eng.* 2021;224:109171. doi:10.1016/J.COMPOSITESB.2021.109171
16. Zhang H, Fan X, Chen W, et al. A simple and green strategy for preparing flexible thermoplastic polyimide foams with exceptional mechanical, thermal-insulating properties, and temperature resistance for high-temperature lightweight composite sandwich structures. *Compos B Eng.* 2022;228:109405. doi:10.1016/J.COMPOSITESB.2021.109405
17. Smeets BJR, Fagan EM, Matthews K, et al. Structural testing of a shear web attachment point on a composite lattice cylinder for aerospace applications. *Compos B Eng.* 2021;212:108691. doi:10.1016/J.COMPOSITESB.2021.108691
18. Dong K, Panahi-Sarmad M, Cui Z, Huang X, Xiao X. Electro-induced shape memory effect of 4D printed auxetic composite using PLA/TPU/CNT filament embedded synergistically with continuous carbon fiber: A theoretical & experimental analysis. *Compos B Eng.* 2021;220:108994. doi:10.1016/J.COMPOSITESB.2021.108994
19. Utekar S, v K S, More N, Rao A. Comprehensive study of recycling of thermosetting polymer composites – Driving force, challenges and methods. *Compos B Eng.* 2021;207:108596. doi:10.1016/J.COMPOSITESB.2020.108596
20. Quan C, Han B, Hou Z, Zhang Q, Tian X, Lu TJ. 3d printed continuous fiber reinforced composite auxetic honeycomb structures. *Compos B Eng.* 2020;187:107858. doi:10.1016/J.COMPOSITESB.2020.107858
21. Li T, Wang L. Bending behavior of sandwich composite structures with tunable 3D-printed core materials. *Compos Struct.* 2017;175:46-57. doi:10.1016/J.COMPSTRUCT.2017.05.001
22. Ye G, Bi H, Hu Y. Compression behaviors of 3D printed pyramidal lattice truss composite structures. *Compos Struct.* 2020;233:111706. doi:10.1016/J.COMPSTRUCT.2019.111706
23. Xu J, Wu Y, Wang L, et al. Compressive properties of hollow lattice truss reinforced honeycombs (Honeytubes) by additive manufacturing: Patterning and tube alignment effects. *Mater Des.* 2018;156:446-457. doi:10.1016/J.MATDES.2018.07.019
24. Khan SF, Zakaria H, Chong YL, Saad MAM, Basaruddin K. Effect of infill on tensile and flexural strength of 3D printed PLA parts. In: *IOP Conference Series: Materials Science and Engineering*. Vol 429. Institute of Physics Publishing; 2018:012101. doi:10.1088/1757-899X/429/1/012101
25. Bragagnolo G, Crocombe AD, Ogin SL, et al. Investigation of skin-core debonding in sandwich structures with foam cores. *Mater Des.* 2020;186:108312. doi:10.1016/j.matdes.2019.108312
26. Majumdar P, Srinivasagupta D, Mahfuz H, Joseph B, Thomas MM, Christensen S. Effect of processing conditions and material properties on the debond fracture toughness of foam-core sandwich composites: Experimental optimization. *Compos Part A Appl Sci Manuf.* 2003;34(11):1097-1104. doi:10.1016/S1359-835X(03)00207-0
27. Chen Q, Linghu T, Gao Y, et al. Mechanical properties in glass fiber PVC-foam sandwich structures from different chopped fiber interfacial reinforcement through vacuum-assisted resin transfer molding (VARTM) processing. *Compos Sci Technol.* 2017;144:202-207. doi:10.1016/j.compscitech.2017.03.033
28. Wang Z, Li Z, Xiong W. Experimental investigation on bending behavior of honeycomb sandwich panel with ceramic tile face-sheet. *Compos B Eng.* 2019;164(August 2018):280-286. doi:10.1016/j.compositesb.2018.10.077

29. Dongyang Cao, Sadeq Malakooti, Vijay N. Kulkarni, Yao Ren, Yingjian Liu, Xu Nie, Dong Qian, D.Todd Griffith HL. The Effect of Resin Uptake on the Flexural Properties of Compression Molded Sandwich Composites. *Wind Energy*. Published online 2021:4-11.
30. Stoll F. Blade Cost and Weight Reduction using TYCOR W engineering cores. In: *2010 Wind Turbine Blade Workshop*. WebCore Technologies; 2010:20-25.
31. Corbridge DM, Harper LT, De Focatiis DSA, Warrior NA. Compression moulding of composites with hybrid fibre architectures. *Compos Part A Appl Sci Manuf*. 2017;95:87-99. doi:10.1016/j.compositesa.2016.12.018
32. Kedari VR, Farah BI, Hsiao KT. Effects of vacuum pressure, inlet pressure, and mold temperature on the void content, volume fraction of polyester/e-glass fiber composites manufactured with VARTM process. *J Compos Mater*. 2011;45(26):2727-2742. doi:10.1177/0021998311415442
33. Truxel A, Avileés F, Carlsson LA, Grenestedt JL, Millay K. Influence of face/core interphase on debond toughness of foam and balsa cored sandwich. *Journal of Sandwich Structures and Materials*. 2006;8(3):237-258. doi:10.1177/1099636206062570
34. ASTM International. *ASTM C393-Standard Test Method for Flexural Properties of Sandwich Constructions.*; 2008. doi:10.1520/mnl10913m
35. ASTM International. *ASTM D790 - 17 Standard Test Methods for Flexural Properties of Unreinforced and Reinforced Plastics and Electrical Insulating Materials*. Published 2017. Accessed May 3, 2021. <https://www.astm.org/Standards/D790>
36. Şener Ö, Dede O, Atalay O, Atasoy M, Kayran A. Evaluation of Transverse Shear Moduli of Composite Sandwich Beams Through Three-Point Bending Tests. *ASME International Mechanical Engineering Congress and Exposition, Proceedings (IMECE)*. 2019;9. doi:10.1115/IMECE2018-87636
37. ASTM D2344 / D2344M - 16 Standard Test Method for Short-Beam Strength of Polymer Matrix Composite Materials and Their Laminates. Accessed November 6, 2021. <https://www.astm.org/Standards/D2344.htm>
38. DIVINYCELL. Datasheet: Mechanical properties of DIVINYCELL H. Published online 2022.
39. Divinycell D. TECHNICAL CHARACTERISTICS DIVINYCELL ® PN PHYSICAL CHARACTERISTICS DIVINYCELL ® PN. Published online 2021.
40. 3A Composite. Datasheet: BALTEK ® SBC. Published online 2022. Accessed September 23, 2022. www.3ACcorematerials.com
41. CEL Components. Datasheet: Nomex Aeronautical grade - CEL Components. Published 2022. Accessed September 23, 2022. <https://www.honeycombpanels.eu/en/products/honeycomb/nomex-aeronautical-grade-en>
42. Hexcel. Datasheet: HexWeb ® Aluminum Flex-Core ® Formable Aluminum Honeycomb. Published online 2017.
43. Saertex. Saertex® 955 g/m² (28 oz/yd²) Stitched Unidirectional, 50". *Technical Data Sheet*. 2020;2:45309.
44. BALSASUD®. BALSASUD® Core Balsa core resin uptake - Product Data Sheet. Published online 2000:727248.
45. Griffith DT, Ashwill TD. The Sandia 100-meter All-glass Baseline Wind Turbine Blade : SNL100-00. *Baseline*. 2011;(June):1-67.

46. Todd Griffith D. *SANDIA REPORT The SNL100-01 Blade: Carbon Design Studies for the Sandia 100-Meter Blade.*; 2013. Accessed May 3, 2021. <http://www.ntis.gov/help/ordermethods.asp?loc=7-4-0#online>
47. Griffith D, Richards PW. *The SNL100-03 Blade: Design Studies with Flatback Airfoils for the Sandia 100-Meter Blade.*; 2014. doi:10.2172/1159116
48. Griffith DT. The SNL100-02 Blade : Advanced Core Material Design Studies for the Sandia 100- meter Blade. *Sand2013-10162*. 2013;(November).
49. Pirouzfard S, Zeinedini A. Effect of geometrical parameters on the flexural properties of sandwich structures with 3D-printed honeycomb core and E-glass/epoxy Face-sheets. *Structures*. 2021;33:2724-2738. doi:10.1016/J.ISTRUC.2021.06.033
50. Ridwan M, Nurgesang FA, Riza R, Syafi'i NM. Mechanical Properties of Sandwich Composite using Glass Fiber Reinforced Polymer as A Skin and 3D Printed Polylactic Acid as A Core. *Journal of Mechanical Engineering, Science, and Innovation*. 2022;2(1):44-54. doi:10.31284/j.jmesi.2022.v2i1.2935
51. Azzouz L, Chen Y, Zarrelli M, et al. Mechanical properties of 3-D printed truss-like lattice biopolymer non-stochastic structures for sandwich panels with natural fibre composite skins. *Compos Struct*. 2019;213:220-230. doi:10.1016/J.COMPSTRUCT.2019.01.103
52. Monti A, EL Mahi A, Jendli Z, Guillaumat L. Quasi-static and fatigue properties of a balsa cored sandwich structure with thermoplastic skins reinforced by flax fibres. *Journal of Sandwich Structures and Materials*. 2019;21(7):2358-2381. doi:10.1177/1099636218760307/ASSET/IMAGES/LARGE/10.1177_1099636218760307-FIG2.JPEG
53. Awad ZK, Aravinthan T, Manalo A. Geometry effect on the behaviour of single and glue-laminated glass fibre reinforced polymer composite sandwich beams loaded in four-point bending. *Mater Des*. 2012;39:93-103. doi:10.1016/J.MATDES.2012.02.023